Rare earth elements as indicators of hydrothermal processes within the East Scotia subduction zone system

Catherine S. Cole[1,2]*, Rachael H. James[1,3], Douglas P. Connelly[3], Ed C. Hathorne[4]

**Corresponding author*

[1]*Ocean and Earth Science, University of Southampton Waterfront Campus, European Way, Southampton, SO14 3ZH, UK*

[2]*Now at Earth and Environmental Sciences, University of St Andrews, Irvine Building, St Andrews, KY16 9AL, UK*

Telephone: +44 1334 463949

E-mail address: csc5@st-andrews.ac.uk

[3]*National Oceanography Centre, University of Southampton Waterfront Campus, European Way, Southampton, SO14 3ZH, UK*

[4]*GEOMAR, Helmholtz Centre for Ocean Research, Kiel, Germany*

Article details: Cole, C. S., James, R. H., Connelly, D. P., Hathorne, E. C. (2014). Rare earth elements as indicators of hydrothermal processes within the East Scotia subduction zone system. *Geochim. et Cosmochim. Acta*, 140. 20-38. DOI:10.1016/j.gca.2014.05.018

Abstract

The East Scotia subduction zone, located in the Atlantic sector of the Southern Ocean, hosts a number of hydrothermal sites in both back-arc and island-arc settings. High temperature (> 348 °C) 'black smoker' vents have been sampled at three locations along segments E2 and E9 of the East Scotia back-arc spreading ridge, as well as 'white smoker' (< 212 °C) and diffuse (< 28 °C) hydrothermal fluids from within the caldera of the Kemp submarine volcano. The composition of the endmember fluids (Mg = 0 mmol/kg) is markedly different, with pH ranging from <1 to 3.4, [Cl^-] from ~90 to 536 mM, [H_2S] from 6.7 to ~200 mM and [F^-] from 35 to ~1000 μM. All of the vent sites are basalt- to basaltic andesite-hosted, providing an ideal opportunity for investigating the geochemical controls on rare earth element (REE) behaviour. Endmember hydrothermal fluids from E2 and E9 have total REE concentrations ranging from 7.3 – 123 nmol/kg, and chondrite-normalised distribution patterns are either light REE-enriched (La_{CN}/Yb_{CN} = 12.8 – 30.0) with a positive europium anomaly (Eu_{CN}/Eu^*_{CN} = 3.45 – 59.5), or mid REE-enriched (La_{CN}/Nd_{CN} = 0.61) with a negative Eu anomaly (Eu_{CN}/Eu^*_{CN} = 0.59). By contrast, fluids from the Kemp Caldera have almost flat REE patterns (La_{CN}/Yb_{CN} = 2.1 – 2.2; Eu_{CN}/Eu^*_{CN} = 1.2 – 2.2).

We demonstrate that the REE geochemistry of fluids from the East Scotia back-arc spreading ridge is variably influenced by ion exchange with host minerals, phase separation, competitive complexation with ligands, and anhydrite deposition, whereas fluids from the Kemp submarine volcano are also affected by the injection of magmatic volatiles which enhances the solubility of all the REEs. We also show that the REE patterns of anhydrite deposits from Kemp differ from those of the present-day fluids, potentially providing critical information about the nature of hydrothermal activity in the past, where access to hydrothermal fluids is precluded.

1. INTRODUCTION

The chemical properties of the rare earth elements (REEs) are fundamentally similar, and differences in their behaviour in natural materials and fluids can usually be attributed to atomic radii controls on their speciation and mobility (Elderfield *et al.*, 1988). In hydrothermal environments, the distribution of the REEs provides important information about fluid evolution during subsurface circulation (Elderfield *et al.*, 1988; Haas *et al.*, 1995), sources of fluid constituents and the extent of seawater mixing (Van Dover, 2000; Embley *et al.*, 2007; Craddock *et al.*, 2010), conditions of mineral deposition and venting history (Craddock and Bach, 2010) and the transport and fate of plume particulate material (German *et al.*, 1990; Bau and Dulski, 1999; Sherrell *et al.*, 1999).

Most hydrothermal fluids have remarkably uniform chondrite-normalised REE (REE_{CN}) distribution patterns, with enrichment in the light-REEs relative to the heavy-REEs and a positive europium anomaly (Michard and Albarède, 1986). This pattern has been observed in fluids from basalt-hosted hydrothermal systems on the Mid-Atlantic Ridge (MAR) (Mitra *et al.*, 1994; James *et al.*, 1995) and the East Pacific Rise (EPR) (Michard *et al.*, 1983; Michard and Albarède, 1986), but also in fluids venting through basaltic andesite and andesite substrates in the Lau Basin (Douville *et al.*, 1999), heavily-sedimented ridges such as the Guaymas Basin and Escanaba Trough (Klinkhammer *et al.*, 1994), and ultramafic-hosted vent systems including Rainbow (Douville *et al.*, 2002). This REE_{CN} pattern has been attributed to exchange of REEs during plagioclase recrystallisation (Campbell *et al.*, 1988; Klinkhammer *et al.*, 1994), but more recent studies suggest that the REEs in hydrothermal fluids are largely derived from alteration minerals (Bach and Irber, 1998; Allen and Seyfried, 2005; Shibata *et al.*, 2006), with their relative distributions determined by the type and concentration of REE ligands (Bau, 1991; Douville *et al.*, 1999; Bach *et al.*, 2003; Allen and Seyfried, 2005; Craddock *et al.*, 2010).

It is now clear however that, under some circumstances, REE distribution patterns in hydrothermal fluids can differ from that described above. At 5 ºS on the MAR, fluids venting close to the critical point of seawater have extremely high REE concentrations, are enriched in the mid-REEs, and have a negative Eu anomaly (Schmidt *et al*., 2010). A recent study of hydrothermal fluids from the Manus back-arc basin has also revealed a wide range of REE_{CN} distribution patterns, from fluids that are enriched in the heavy REE elements, to fluids with relatively flat REE_{CN} patterns (Craddock *et al.,* 2010). These different distribution patterns are attributed to differences in REE solubility due to variations in the relative abundance and stability of REE-chloride, fluoride and sulphate complexes as a function of fluid temperature, pH and ligand concentration. To this end, these authors suggest that the REEs can be used as tracers for input of fluoride- and sulphur-rich magmatic volatiles in seafloor hydrothermal fluids.

To test whether variable REE_{CN} patterns are characteristic of arc and back-arc environments, we have determined REE concentrations in hydrothermal fluids and chimney sulphates recovered from newly-discovered vent sites in the East Scotia subduction zone system (Rogers *et al.*, 2012). Two sites (E2 and E9) are located on the East Scotia Ridge (ESR) back-arc spreading ridge; the other is a recently erupted submarine volcano (Kemp Caldera) that forms part of the South Sandwich Island volcanic arc. The chemical composition and temperature of the hydrothermal fluids differs significantly between the sites (German *et al.*, 2000; Rogers *et al.*, 2012; James *et al.*, in review), allowing us to examine the controls on REE abundances and REE_{CN} distribution patterns. We show that the REEs can provide key information as to subsurface hydrothermal processes in back-arc and island-arc systems such as fluid-rock interaction, phase separation, secondary-mineral dissolution, and magmatic gas injection. Further, we show that deposits of anhydrite can preserve past fluid compositions and consequently record changes in hydrothermal and magmatic regimes.

2. GEOLOGIC SETTING AND VENT CHEMISTRY

2.1 East Scotia Ridge

The East Scotia Ridge (ESR) is an isolated inter-oceanic back-arc spreading centre associated with subduction of the South American plate beneath the overriding Sandwich plate in the East Scotia Sea, Southern Ocean (Figure 1) (Barker, 1970; German *et al.*, 2000). Spreading was initiated between the Scotia and Sandwich plates > 15 Ma ago (Larter *et al.*, 2003), and current spreading rates vary between 60-70 mm y^{-1} along the ridge (Thomas *et al.*, 2003). Despite its intermediate spreading rate, the ESR has an axial morphology more typical of a slow spreading ridge (Leat *et al.*, 2000). Deep median valleys, associated with most of the ridge segments, are attributed to reduced mantle temperature and melt production by subduction-related conduction and convection (Livermore *et al.*, 1994; 1997).

The ESR consists of nine ridge segments (E1-E9), separated by non-transform faults (Livermore *et al.*, 1994). Segments E2 and E9 are distinct in that they possess magmatically inflated axial highs, more characteristic of fast-spreading ridges (Leat *et al.*, 2000; Bruguier and Livermore, 2001). Locally enhanced melting and magma production is evident from the seismically imaged melt lens beneath E2 and that postulated to exist beneath E9 (Leat *et al.*, 2000). Eastward tearing of the South American plate, as suggested from intense seismic activity at 50-130 km depth beneath the northern ESR (Brett, 1977), may facilitate mantle flow from the South Atlantic around the edges of the subducting slab, feeding these axial magma chambers. Mantle flow by displacement may also be important as a result of the rapid eastward rollback of the South Sandwich Trench (Pelayo and Wiens, 1989; Bruguier and Livermore, 2001). The enriched volatile flux derived from dehydration of the sinking plate may also be responsible for the observed melt anomalies (Livermore *et al.*, 1997).

99 The dominant crustal lithology of the ESR is basalt to basaltic andesite, with limited
100 subduction influence (Leat *et al.*, 2000, 2004; Fretzdorff *et al*., 2002). Radiogenic isotope
101 analysis of basalts from the summit of E2 compared with the segment ends indicates the
102 presence of an enriched mantle source beneath the axial volcanic ridge (AVR), characteristic
103 of a mantle plume (Leat *et al.*, 2000). Whilst seismic profiles have revealed a highly focused,
104 shallow melt body beneath the AVR of E2, no melt reservoir has been imaged beneath E9
105 (Bruguier and Livermore, 2001). However, a large axial summit caldera, the 'Devil's
106 Punchbowl', is thought to represent collapse associated with magma withdrawal, suggesting
107 that a magma chamber has existed beneath this ridge segment in the past (Bruguier and
108 Livermore, 2001).

109 Hydrothermal plumes were first detected above segments E2 and E9 of the ESR in
110 1998 from geochemical surveys of the water column (German *et al.*, 2000). In 2009, active,
111 high-temperature 'black smoker' vents were observed for the first time using a deep-towed
112 camera system, and these were subsequently sampled by the remotely operated vehicle
113 (ROV) *ISIS* during RRS *James Cook* cruise 42 in early 2010 (Rogers *et al.*, 2012).

114 The E2 hydrothermal site is located just south of the AVR, between 56˚5.2′ and
115 56˚5.4′ S and between 30˚19.0' and 30˚19.35′ W at ~2600 m water depth. 'Dog's Head'
116 consists of a series of four chimneys, up to ~10 m high, that actively vent black smoker fluids
117 at temperatures of up to 351 °C. The 'Sepia' vent site lies 75 m to the south east of Dog's
118 Head, and chimneys up to ~10 m high vent fluids at temperatures of up to 353 ˚C. The
119 chloride concentration ($[Cl^-]$) of the endmember fluids (532 - 536 mM) is close to local
120 bottom seawater (540 mM) and the lowest recorded fluid pH is 3.02 (James *et al.*, in review).
121 Sulphate behaves conservatively during seawater mixing and extrapolates to a near-zero
122 concentration in endmember fluids (0.97 - 1.31 mM). Concentrations of H_2S and fluoride in
123 the endmember fluids (respectively, 6.7 – 7.1 mM and ~39 μM) are typical of basalt-hosted

mid-ocean ridge systems (Von Damm, 1990; Kelley *et al.*, 2002), suggesting that input of magmatic volatiles is negligible (James *et al.*, in review).

There are two sites of high temperature hydrothermal activity at E9, located between 60° 02.5' and 60° 03.0' S and between 29° 59.0' and 29° 58.6' W at ~2400 m water depth. At the northern site, fluids issue from the ~10 m high 'Black & White' chimney at temperatures of up to 383 ˚C. At the southern site, high temperature fluids (348 – 351 ˚C) are expelled from three chimney structures. 'Ivory Towers' is located to the north of the site, and emits high temperature fluids through a number of exits, including clusters of 'beehive' diffusers. Approximately 50 m to the south of Ivory Towers two further structures, 'Pagoda' and 'Launch Pad', occur in close proximity. In contrast to E2, the chloride concentration of the E9 fluids is distinctly lower than local bottom seawater, ranging from 98.2 mM at Black & White, to 179 mM at Launch Pad and 220 mM at Ivory Towers and Pagoda. This is attributed to phase separation of the fluids (James *et al.*, in review); note that the temperature of the Black & White fluids lies on the two-phase boundary for seawater at this depth (Bischoff and Rosenbauer, 1984). As a consequence, concentrations of H_2S in the endmember fluids are higher (9.5 – 14 mM) than they are in the higher-Cl fluids from E2. The pH (3.08 – 3.42) and fluoride (34.6 – 54.4 μM) concentrations of the endmember fluids are similar to E2, again indicating that input of magmatic volatiles is negligible (James *et al.*, in review). Sulphate concentrations of endmember fluids from the southern sites (Launch Pad, Ivory Tower and Pagoda) are close to zero (0.25 ± 0.71 mM), but considerably higher at Black & White (3.57 mM). This suggests that Black & White fluids are affected by input of anhydrite, either because of entrainment of chimney material during sampling, or dissolution of material precipitated at lower temperatures in the subsurface and subsequent incorporation into the venting fluids (James *et al.*, in review).

2.2 South Sandwich Island Arc

The South Sandwich Island Arc is an intra-oceanic, volcanic arc associated with the subduction of the southernmost South American plate beneath the Sandwich plate (Larter *et al.*, 2003). Basement crust here is young (8 – 10 Ma), generated by back-arc spreading at the ESR and has a thickness of 16 - 20 km (Leat *et al.*, 2004). The arc consists of seven main islands (up to 3 km from seafloor to summit) and several smaller islands and seamounts varying in composition from basaltic to rhyolitic (Leat *et al.*, 2004). Kemp Seamount is a volcanically active, submerged component of the southern part of the arc, located ~50 km west-south-west of Thule Island and ~70 km north of the southern subducting edge. The dominant crustal lithology of Kemp is tholeiitic basalt and basaltic andesite, but high concentrations of Nd, and high $^{87}Sr/^{86}Sr$, Nd/Hf and Ba/Th ratios indicate a strong subduction component, although there is minimal sediment-melt influence (Leat *et al.*, 2004). Hydrothermal activity was discovered within a submarine volcanic crater to the west of Kemp Seamount (59° 42'S and 28° 18.59'W), at a water depth of ~ 1420m, in 2009. White smoker-type fluids issue from friable chimney structures at temperatures of up to 212 °C to the west of the centre of the caldera, at a site named 'Winter Palace'. Low temperature (< 28 °C) diffuse fluids issue through a seafloor fissure at another site, called Great Wall, ~ 100 m to the northwest of Winter Palace. Sulphur-rich minerals precipitate from the fluids, forming a ~50 cm high 'wall' along the fissure. The floor of the caldera is currently covered with sulphur and ash deposits, suggesting that there has been a recent volcanic blow-out event (de Ronde *et al*., 2011; Leybourne *et al*., 2012).

Although no vent fluids with very low [Mg] were collected from Kemp (Section 4.1), the chloride concentration of endmember fluids is likely to be low (90 ± 37 mM). The endmember fluids also appear to have very high levels of H_2S (200 ± 15 mM) and fluoride (1000 ± 110 μM), and low pH (1 ± 1). This strongly suggests that the fluids are phase

separated, and they are affected by input of magmatic volatiles (Powell *et al*., 2011). The fluids also appear to have been affected by deposition of anhydrite in the subsurface, as sulphate concentrations extrapolate to negative values (-8 ± 3 mM) at zero [Mg].

3. METHODS

3.1 Sample Collection and Preparation

3.1.1 Focused and diffuse fluids

Focused and diffuse vent fluids were collected by ROV *ISIS* from E2, E9 and Kemp Caldera in 2010 during RRS *James Cook* cruise JC42. Titanium syringe samplers, equipped with an inductively coupled link (ICL) temperature sensor at the nozzle tip, were inserted into the chimney orifice to collect focused vent fluids. Diffuse fluids were collected using a specially-constructed diffuse sampler, consisting of a pseudo venture tube, constructed in titanium, fitted with a heat-resistant weighted 'skirt' at its base to form a seal with the seafloor. The diffuse sampler was placed over the target area, and fluids were sampled by insertion of a Ti syringe into the top of the tube. Entrainment of ambient seawater was minimised by delaying syringe activation until a constant temperature reading was observed. Back onboard, the fluids were transferred to acid-cleaned 1L HDPE bottles, and any solid material ('dregs') that had presumably precipitated as the sample cooled was rinsed from the Ti samplers into a 30ml acid-cleaned HDPE bottle. All samples were acidified to pH 2 using thermally distilled (TD) HNO_3.

Onshore, fluid samples were filtered through a polycarbonate membrane filter (0.2 μm; Whatman) to separate any particles that had precipitated during storage. The filtrate was diluted with 2% HNO_3 for analysis of major elements. Particulate material retained on the filters was dissolved in 50% TD HNO_3 at 60 °C for several days, and then transferred to a

198 microwave digestion vessel and microwaved at 400W for 3 minutes. This step was repeated
199 as necessary until the filter had completely dissolved. The digested sample was then
200 transferred to a 15 mL Savillex vial with Milli-Q water, and evaporated to dryness. Finally,
201 the sample was dissolved in 10 mL of 1.6M HNO_3 and its mass was determined. The 'dregs'
202 were filtered, dissolved, dried-down and re-dissolved in the same way. The concentration of
203 the REEs was determined in each fraction (Section 3.2), and the overall composition of the
204 vent fluids was reconstructed (Table 1).

205 ***3.1.2 Chimney samples***

206 Samples of the uppermost section of the vent chimneys from Dog's Head (E2), Black
207 & White, Ivory Towers and Launch Pad (E9) and Winter Palace (Kemp Caldera) were taken
208 using the ROV manipulator arm and transferred to the ROV basket. Back on board the ship,
209 the samples were photographed and their dimensions noted. Onshore, individual grains of
210 anhydrite were handpicked from cut cross sections through the chimney wall using a
211 binocular microscope. Mineral identification was confirmed by X-ray diffraction (Philips
212 X'Pert pro XRD) at the National Oceanography Centre, Southampton.

213 **3.2 Analytical Methods**

214 ***3.2.1. REE concentration of fluids***

215 Rare earth element concentrations in filtered fluid samples were determined by
216 inductively coupled plasma mass spectrometry (ICP-MS; Agilent 7500) at GEOMAR, Kiel,
217 using a SeaFast system for online matrix-removal and pre-concentration of the REEs
218 following the method of Hathorne *et al.*, (2012). Based on replicate analyses (n = 8) of a
219 well-characterised seawater sample from 2000 m depth in the Southern Ocean (Circumpolar
220 Deep Water (CDW) sample ts PS71 131-1; (Hathorne *et al.*, 2012; Stichel *et al.*, 2012)), the
221 external reproducibility of this method at the 95% confidence level (2σ) is < 10% for La – Pr,

Eu, Dy – Lu; 11 – 17% for Nd, Sm, Yb, Tb and < 22% for Gd. The accuracy of this technique has been demonstrated in an inter-laboratory comparison exercise (van de Flierdt *et al.*, 2012).

The REE content of the particulate and dregs fractions was determined by ICP-MS (Thermo Fisher Scientific ELEMENT) at the National Oceanography Centre in Southampton. Single-element standards of Ba, Ce, Pr and Sm (Inorganic Ventures) were analysed alongside the samples to enable interference corrections to be made on Eu and the heavy REEs. Samples were calibrated against a set of five rock standards; BIR-1 and BHVO-2 (US Geological Survey), and JB-3, JA-2, JGb-1 (Geological Survey of Japan). Instrument drift was assessed by addition of internal standards (In and Re). Based on duplicate analyses of the rock standards, the external reproducibility (2σ) of this technique is < 5% for La – Sm and Dy - Lu; < 8% for Eu and Tb and < 16% for Gd.

3.2.2 REE concentration of anhydrite

A minimum of 10 mg of anhydrite was dissolved in ~5 ml of Milli-Q water and a drop of 50% TD HNO_3 by heating on a hotplate at 60 °C for several days. Once dissolved, the anhydrite sample was transferred into a 20 ml acid-cleaned LDPE bottle. A volume of fluid equivalent to 6 mg of anhydrite was sub-sampled, dried down and re-dissolved in 4 ml of 3% TD HNO_3 spiked with 10 ppb In, Re, and 20 ppb Be as internal standards. Concentrations of the REEs, Y, and major cations (Ba, Ca, Sr) were determined by ICP-MS (Thermo Scientific X-Series) at the National Oceanography Centre, Southampton, calibrated against five rock standards; BIR-1 and BHVO-2 (US Geological Survey), and JB-3, JA-2, JGb-1 (Geological Survey of Japan), as well as matrix-matched synthetic standards. The external reproducibility (2σ) of these analyses was < 4% for all of the REEs, based on duplicate analyses of the rock standards. The concentration of REEs in anhydrite was

246 calculated by normalising to the mass of anhydrite, determined by the measured calcium
247 concentration. Anhydrite is assumed to be the only source of REEs in each sample.

248 ***3.2.3 Sr isotope composition of fluids and anhydrite***

249 $^{87}Sr/^{86}Sr$ ratios of both the vent fluids and anhydrite were determined by thermal
250 ionisation mass spectrometry (TIMS; VG Sector 54) at the National Oceanography Centre,
251 Southampton. Sr was separated from a sub-sample of fluid or dissolved anhydrite containing
252 ~1 μg of Sr by cation-exchange chromatography using Sr-spec resin (Eichrom). Matrix
253 elements were eluted with 3M TD HNO_3, and the Sr fraction was collected in Milli-Q water,
254 then dried down, re-dissolved in 1.5 μl of 1M TD HCl, and loaded with a Ta activator
255 solution onto single Ta filaments. Analyses of the NIST987 Sr isotope standard, measured
256 over the course of this work, give $^{87}Sr/^{86}Sr$ ratios of 0.710245 ± 0.000020 (2σ, n = 3), within
257 error of the certified value (0.710250; National Institute of Standards and Technology).

258 **4. RESULTS**

259 **4.1 REE Composition of Hydrothermal Fluids**

260 Results of REE analyses of the fluids with lowest Mg recovered from each vent site
261 are reported in Table 1. Of the samples collected from E2 and E9, all but 2 contain <5
262 mmol/kg Mg and thus consist of <10% bottom seawater. The zero-Mg endmember
263 concentrations for these vents are calculated, as is the usual practise, by extrapolating from
264 the composition of bottom seawater through the Mg concentration measured in samples from
265 a given vent, to zero-Mg. Endmember concentrations are given in Table 1.

266 Fluids recovered from Kemp Caldera have much higher levels of Mg (> 43 mM).
267 This is almost certainly due to mixing with seawater during the sampling procedure. To this
268 end, the temperature of the vent fluids measured using the ICL probe (~212 ˚C) was
269 significantly higher than that recorded when the fluid was sampled (< 28 ˚C), as a result of

break-up of the friable chimney. Thus, although endmember fluids with Mg > 0 have been reported for some back-arc basin vents (e.g. Douville *et al*., 1999; Craddock *et al*., 2010), this scenario is unlikely to apply here. Because the REEs do not behave conservatively during mixing with seawater, due to coprecipitation with iron and manganese (oxy)hydroxides and anhydrite (German *et al.*, 1990; Bau and Dulski, 1999; Sherrell *et al.*, 1999), it is not possible to accurately estimate the REE composition of the vent fluid endmember. For this reason, all subsequent discussion of the Kemp Caldera fluids will focus on REE_{CN} distribution patterns rather than absolute concentrations.

The total REE concentration (∑REE) of ESR endmember fluids varies from 30 - 40 nmol/kg at E2, to 123 nmol/kg at E9 North, and 7.3 - 8.2 nmol/kg at E9 South. This compares to a ∑REE value of 0.1 nmol/kg for Circumpolar Deep Water (Hathorne *et al.*, 2012).

REE distribution patterns, normalised to chondrite using values given in Taylor and McClennan (Taylor and McClennan, 1985), are presented in Figure 2 together with representative patterns for fluids from basalt-hosted mid-ocean ridge systems (MAR: TAG, Lucky Strike, Two Boats; EPR: 13 °N, 17-19 °S), the Lau back-arc basin (Vai Lili), and the Manus back-arc basin (DESMOS, North Su, Suzette, Satanic Mills, Snowcap), as well as Southern Ocean seawater from 2000 m depth. Three distinct REE_{CN} patterns can be identified in fluids from the East Scotia Sea. Endmember fluids from E2 and E9 South are enriched in the light REEs (La_{CN}/Yb_{CN} = 25.2 and 30.0 for Dog's Head and Sepia, and 17.2, 14.9 and 21.8 for Ivory Towers, Pagoda and Launch Pad, respectively; Table 2) and have a positive europium anomaly (Eu_{CN}/Eu^*_{CN} = 3.45 and 3.84 for Dog's Head and Sepia, and 14.3, 50.9 and 59.5 for Ivory Towers, Pagoda and Launch Pad, respectively). By contrast, endmember fluids from E9 North are enriched in the middle REEs (La_{CN}/Nd_{CN} = 0.61; Nd_{CN}/Yb_{CN} = 21.0), and have a negative Eu anomaly (Eu_{CN}/Eu^*_{CN} = 0.59). They also have

295 extremely high REE concentrations (∑REE = 123 nmol/kg). Finally, white smoker and
296 diffuse fluids sampled from the Kemp Caldera have almost flat REE patterns, with
297 La_{CN}/Yb_{CN} = 2.1 – 2.2 and Eu_{CN}/Eu^*_{CN} = 1.2 – 2.2.

298 **4.2 $^{87}Sr/^{86}Sr$ Composition of Vent Fluids**

299 The Sr isotopic composition of the endmember hydrothermal fluids is calculated by
300 extrapolating measured values to (Mg/Sr) = 0. Lowest $^{87}Sr/^{86}Sr$ values were obtained for
301 fluids from Sepia (E2; 0.704035), with more radiogenic ratios observed in fluids from Black
302 & White at E9 North (0.705762), Ivory Tower (0.704610), Launch Pad (0.705014), and
303 Pagoda (0.704890) at E9 South (Table 1). These values are similar to those measured in
304 fluids from other back-arc spreading systems, such as Lau Basin (0.7044 – 0.7056) and
305 Manus Basin (0.70425 – 0.70435) (Fouquet *et al.*, 1991; Mottl *et al.*, 2011; Reeves *et al.*,
306 2011), and are higher than typical mid-ocean ridge fluids, such as TAG and 21°N EPR
307 (0.7029 – 0.7034) (Palmer, 1992; Gamo *et al.*, 1996).

308 **4.3 REE Composition of Chimney Anhydrites**

309 The REE-Y compositions of chimney anhydrites sampled from some of the sites on
310 the ESR and within the Kemp Caldera are presented in Table 3. Total REE abundance in
311 anhydrite is much higher in chimney samples recovered from E9 North (24.3 ppm) than at
312 any of the other vent sites (4.75 – 9.13 ppm at E2, 0.33 – 5.44 ppm at E9 South, and 0.61 –
313 5.19 ppm at Winter Palace, Kemp Caldera) (Table 4). At all sites, ∑REE is far higher for
314 anhydrite than for the endmember hydrothermal fluids, by a factor of up to 1600 at E2, 1400
315 at E9 North and 4600 at E9 South. Differences in ∑REE between sites are mainly related to
316 differences in the extent of seawater mixing in fluids from which the anhydrite precipitates
317 (Table 4). The extent of seawater mixing can be calculated from $^{87}Sr/^{86}Sr$ ratios by mass
318 balance (Bach *et al.*, 2005):

$$\% \text{ seawater} = \frac{[(R_{HF} \times [Sr]_{HF}) - (R_{anh.} \times [Sr]_{HF})] \times 100}{[((R_{HF} \times [Sr]_{HF}) - (R_{sw} \times [Sr]_{sw}) - R_{anh.}) \times ([Sr]_{HF} - [Sr]_{sw})],}$$

where R is the $^{87}Sr/^{86}Sr$ ratio of endmember hydrothermal fluid (HF), anhydrite (anh.) and seawater (sw), and [Sr] is the concentration of Sr. Most anhydrite precipitates from a fluid consisting of >50% seawater (Table 4), but anhydrite from E9 North, appears to precipitate from a fluid that has undergone very little mixing with seawater, consisting of ~98% vent fluid. This is likely to be an artefact of dissolution of anhydrite affecting the strontium concentration of the hydrothermal fluid, as discussed in Section 5.4.

Chondrite-normalised REE distribution patterns for anhydrite samples from E9 (Figure 3) are similar to those measured in the hydrothermal fluids. Thus, samples from E9 South are enriched in the light REEs (La_{CN}/Yb_{CN} = 16.6 – 26.1; Table 4) and have a positive Eu anomaly (Eu_{CN}/Eu^*_{CN} = 13.9 – 18.8), and samples from E9 North are enriched in the middle REEs (La_{CN}/Nd_{CN} = 0.7; Nd_{CN}/Yb_{CN} = 24.7) and have a small negative Eu anomaly (Eu_{CN}/Eu^*_{CN} = 0.61). Normalisation of REE abundance to the vent fluids generates almost flat REE patterns (with the exception of Launch Pad, where anhydrite is depleted in Eu relative to the fluid), confirming that there is negligible fractionation of the REEs between anhydrite and the vent fluids (Figure 4).

By contrast, the REE_{CN} patterns of anhydrite recovered from E2 (Dog's Head) and Kemp Caldera (Winter Palace) are different from the vent fluid pattern. Like the vent fluids, anhydrite from E2 is enriched in the light REEs (La_{CN}/Yb_{CN} = 14.3 – 21.6), but anhydrite has a negative, rather than a positive, Eu anomaly (Eu_{CN}/Eu^*_{CN} = 0.35 – 0.85). At Kemp Caldera, anhydrite is strongly enriched in the heavy REEs relative to the light REEs (La_{CN}/Yb_{CN} = 0.03 – 0.09), whereas the vent fluids have relatively flat REE_{CN} patterns

342 (Figure 2). As a consequence, the vent fluid-normalised REE pattern for anhydrite from
343 Kemp Caldera shows strong enrichment in the heavy REEs (Figure 4).

5. DISCUSSION

Despite their close proximity, and similar host rock compositions, the REE_{CN} patterns of hydrothermal fluids and chimney anhydrite from the different vent sites are variable. The fluids are also different in terms of their pH, temperature, Cl, H_2S, F and SO_4 concentrations. Accordingly, these vent fluids can be used to identify the key controls on REE solubility in submarine hydrothermal fluids in subduction zone settings.

5.1 Host-Rock Influence

Hydrothermal fluids primarily derive their REE load through high-temperature reaction with the oceanic crust during subsurface circulation and are consequently highly enriched in all REEs compared with seawater (Michard *et al.*, 1983; Klinkhammer *et al.*, 1994). Comprehensive REE data for ESR and Kemp Caldera basalts, from dredge and wax core samples, are reported by Leat *et al*., (2000; 2004) and Fretzdorff *et al*., (2002). Basalts from the AVR of segments E2 and E9 have similar total REE concentrations (respectively, 65 - 78 and 60 - 75 ppm), and they are slightly enriched in the light REEs compared with the heavy REEs (La_{CN}/Yb_{CN} = 1.98 and 1.71). Basalts from Kemp Caldera have lower ∑REE (21 – 25 ppm) and relatively flat REE_{CN} patterns (La_{CN}/Yb_{CN} = 1.00). The relative concentration of the REEs in hydrothermal fluids typically varies systematically with ionic radius, with larger ions preferentially partitioning into solution. Whilst it has been suggested that this reflects crystal-chemical exchange between plagioclase phenocrysts and seawater circulating in the reaction zone (Klinkhammer *et al*., 1994), similar REE distribution patterns are also observed in fluids derived from hydrothermal alteration of ultramafic peridotite, which does not contain plagioclase (Allen and Seyfried, 2005). Further, leaching experiments have shown that REEs in fluids mainly originate from secondary alteration minerals and interstitial material (Bach and Irber, 1998; Shibata et al., 2006), with fluid speciation exerting the dominant control on their relative distributions.

Partition coefficients for the REEs between hydrothermal fluids and basalt are presented for each site on the ESR and for Kemp Caldera in Figure 5. Fractionation of the REEs into fluids at E2 and E9 South increases with ionic radius, in line with the effects of crystal-chemical exchange demonstrated for plagioclase during magma segregation (Campbell *et al.*, 1988; Klinkhammer *et al.*, 1994). By contrast, the middle REE enriched patterns of E9 North vent fluids, and the relatively flat REE patterns of Kemp Caldera vent fluids, cannot be explained by plagioclase leaching, or fractionation due to differences in ionic radius. If exchange reactions are involved, their original REE signatures must be overprinted by other processes.

5.2 Influence of Chlorinity and Phase Separation

The solubility of the REEs is strongly influenced by the availability of anionic ligands, which stabilise these elements in fluids through complexation (Wood, 1990; Gammons *et al.*, 1996; Douville *et al.*, 1999). Chloride is typically a major constituent of hydrothermal fluids and speciation calculations indicate that, at temperatures above 300 °C, 97 - 100 % of all REEs are stabilised as chloride complexes (Gammons *et al.*, 1996; Douville *et al.*, 1999). Chloride forms stronger complexes with the LREEs compared to the HREEs and is likely to be an important driver behind the light REE-enrichment observed in vent fluids from E2 and E9 South on the ESR, and for most mid-ocean ridge hydrothermal systems (Haas *et al.*, 1995; Migdisov *et al.*, 2009).

Endmember vent fluids at E9 South have typical mid-ocean ridge-type REE_{CN} patterns, i.e. they are enriched in the light REEs and have a positive Eu anomaly, but they have very low total REE concentrations, ~5 times lower than those measured at E2, and the Eu anomaly is more than an order of magnitude higher. Because of phase separation, the E9 South vent fluids have extremely low [Cl^-] (179 - 220 mM); thus low ∑REE values likely

393 reflect the reduced availability of chloride ligands for complexation. Note that low [Cl^-] vent
394 fluids from 17-19 °S on the East Pacific Rise also have low ∑REE (Table 2; Figure 2).

395 Although the effects of phase separation on the major-element chemistry of vent
396 fluids have been well studied (Bischoff and Rosenbauer, 1984; Von Damm and Bischoff,
397 1987; Butterfield *et al.*, 1990; Auzende *et al.*, 1996; Charlou *et al.*, 1996; Coumou *et al.*,
398 2009), the effects on REE behaviour are less well known and, to our knowledge, there are no
399 REE data in the literature for very low Cl fluids from subduction zone settings. REE
400 concentrations tend to be higher in chloride-rich brines and lower in low-chloride fluids
401 (Douville *et al.*, 1999; 2002), and low-Cl fluids tend to have larger Eu_{CN}/Eu^*_{CN} anomalies
402 (Douville *et al.*, 1999). Experimentally-determined partition coefficients for Eu between
403 vapour and liquid in a NaCl-H_2O system at the critical point are similar to those for its
404 neighbouring REEs (Shmulovich *et al.*, 2002). However, thermodynamic calculations
405 suggest that Eu is more strongly complexed by ligands including chloride, fluoride and
406 sulphate at 350 °C compared to Gd and Sm (Wood, 1990), and experimental studies have
407 shown that Eu^{2+} builds stronger complexes with chloride relative to the trivalent REEs (Allen
408 and Seyfried, 2005). The fact that the low-Cl fluids at E9 South have a high Eu_{CN}/Eu^*_{CN}
409 anomaly suggests that Eu^{2+} has the strongest affinity for chloride, even when chloride
410 concentrations are low.

411 **5.3 Influence of Magmatic Volatiles**

412 The chemical composition of hydrothermal fluids sampled at Kemp Caldera is
413 markedly different from E2 and E9 fluids. Based on the assumption of a zero-Mg
414 endmember, Kemp Caldera fluids have very high fluoride (~ 1000 μM) and hydrogen
415 sulphide (~ 200 mM) concentrations, and very low pH (1 ± 1). In comparison to the ESR,
416 Kemp Caldera is located in close proximity to the subducting arc, where the entrainment of
417 volatile gases (H_2O, CO_2, SO_2, HCl, HF) into circulating hydrothermal fluids (Reeves *et al.*,

418 2011) is likely to influence pH and the type and availability of anionic ligands (Bai and
419 Koster van Groos, 1999). The distinctive composition of Kemp Caldera hydrothermal fluids,
420 together with the widespread deposition of native sulphur (derived from disproportionation of
421 SO_2; Iwasaki and Ozawa (1960); Gamo *et al*. (1997); Reeves *et al*. (2011)), is indicative of
422 input of magmatically sourced acid volatiles (Powell *et al*., 2011). These acid volatiles
423 provide an additional source of anionic ligands capable of complexing with the REEs.

424 Hydrothermal fluids from mid-ocean ridge settings typically have low $[F^-]$ relative to
425 seawater (Edmond *et al.*, 1979; Von Damm *et al.*, 1985), because mineral phases such as
426 magnesite and magnesium hydroxide sulphate hydrate have a strong affinity for fluoride ions
427 (Seyfried and Ding, 1995). In arc settings, however, the release of HF by magmatic
428 degassing (Aiuppa *et al.*, 2009) can generate fluids with high $[F^-]$ and low pH, resulting in
429 enhanced REE mobility in fluids as observed in the Eastern Manus Basin (Bach *et al.*, 2003;
430 Craddock *et al.*, 2010; Reeves *et al.*, 2011). Our data support this. Extrapolation of the
431 Kemp Caldera fluid sample with lowest [Mg] to zero [Mg], which provides a minimum value
432 for the REE content of the vent fluid endmember (because of precipitation; see Section 4.1),
433 indicates that the endmember ∑REE value of Great Wall fluids is ~ 70 nmol/kg. This value
434 is an order of magnitude higher than it is for fluids from E9 South (~ 8 nmol/kg), which have
435 similarly low $[Cl^-]$, suggesting that input of acid volatiles has significantly enhanced the
436 solubility of the REEs.

437 Input of acid volatiles may also affect REE_{CN} distribution patterns. Fractionation
438 between the LREEs and HREEs (La_{CN}/Yb_{CN}) generally decreases as the abundance of
439 fluoride relative to chloride ($[F^-]/[Cl^-]$) increases (Figure 6). This is because stability
440 constants for complexation of the REEs with chloride are higher for the LREE than the
441 HREEs (Wood, 1990; Migdisov *et al.*, 2009), but this effect is reduced if fluoride
442 concentrations are high. In the Manus Basin, fluids sampled from Suzette and Satanic Mills,

443 which have very high $[F^-]/[Cl^-]$ (0.6 – 0.8 μM/mM), are also highly enriched in the HREEs
444 (Figure 2; Craddock *et al*., 2010). Similarly, fluids venting from the Kemp Caldera may have
445 displayed this pattern of HREE-enrichment in the past, as recorded in anhydrite in Winter
446 Palace chimney material (See Section 5.5). Fluoride complexes of the heavy REEs are
447 predicted to be more stable than those of the light REEs and Eu^{2+} (Wood, 1990), and
448 thermodynamic calculations of species distribution in Manus Basin fluids indicate that the
449 HREEs are predominantly complexed with fluoride in F^--rich solutions (Craddock *et al*.,
450 2010). However experimental data suggest that formation constants for HREE-F complexes
451 in seawater have been significantly overestimated at high (> 150 °C) temperatures (Migdisov
452 *et al.*, 2009). Further, Williams-Jones *et al*. (2012) suggest that fractionation of the LREEs
453 from the HREEs in hydrothermal fluids is primarily controlled by temperature rather than
454 fluid speciation. We note, however, that while these studies support the importance of
455 chloride complexation in REE fractionation in typical MOR-style hydrothermal fluids, they
456 cannot explain the diversity in REE_{CN} patterns measured in vent fluids from Kemp Caldera,
457 or the Manus Basin.

458 Vent fluids from Kemp Caldera, and 'acid-sulphate' fluids from the Manus Basin
459 (Craddock *et al.*, 2010), have low La_{CN}/Yb_{CN} and Eu_{CN}/Eu^*_{CN} values for a wide range of $[F^-]/[Cl^-]$
460 (Figure 6). Speciation calculations by Craddock *et al*. (2010) indicate that
461 complexation exerts a relatively minor influence on REE solubility in acid-sulphate fluids.
462 At low pH, REEs are readily leached from the host rock with minimal fractionation, and are
463 stable in solution as free ions. REE solubility may be further enhanced by complexation with
464 sulphate (e.g. DESMOS), and at higher temperatures (>200 °C) by the formation of REE-Cl
465 complexes (e.g. North Su) (Craddock *et al*., 2010). The relatively flat REE_{CN} distribution
466 patterns for fluids recovered from Kemp Caldera may therefore be characteristic of very low
467 pH fluids.

468

469 **5.4 Influence of Anhydrite**

470 Anhydrite will precipitate in hydrothermal environments at temperatures > 150 °C,
471 due to conductive heating of seawater or as high-temperature fluids mix with seawater.
472 Anhydrite precipitation represents a major sink for rare earth elements in hydrothermal
473 environments (Mills and Elderfield, 1995), and deposits of this mineral within vent chimneys
474 on the ESR and Kemp Caldera are enriched in the REEs by a factor of several thousand
475 relative to hydrothermal fluids.

476 The rare earth element chemistry of hydrothermal fluids can therefore be potentially
477 influenced by anhydrite precipitation and dissolution (Craddock *et al.*, 2010; Schmidt *et al.*,
478 2010). At Black & White (E9 North), vent fluids have very high ∑REE, despite their low
479 chlorinity (Douville *et al.*, 2002), a negative Eu anomaly and, unlike the other vent sites, they
480 exhibit a positive correlation between ∑REE and [Ca] (Figure 7; $R^2 = 0.72$ compared with <
481 0.14 for all other sites). In addition, the sulphate concentration of the endmember fluids is ~4
482 mM, rather than zero as it is in most vent fluids (Von Damm, 1990). All of this suggests that
483 the vent fluids are affected by dissolution of anhydrite, which makes up the inner wall of the
484 Black & White chimneys (James *et al.*, in review). Addition of ~4 mM of SO_4 is equivalent
485 to dissolution of 544 mg anhydrite per kg of vent fluid. We calculate that < 1 g of anhydrite
486 from the Black & White chimneys, added to 1 kg of a vent fluid unaffected by anhydrite
487 dissolution (i.e. the low Cl fluids from E9 South), is sufficient to produce a vent fluid with
488 high ∑REE and a negative Eu anomaly, that is enriched in the middle REEs.

489 REE_{CN} distribution patterns similar to those in Black & White fluids have previously
490 been observed at the 'Two Boats' hydrothermal site at 5 °S on the Mid-Atlantic Ridge
491 (Figure 2; Schmidt *et al.*, 2010). Crucially, the temperature and pressure of the fluids venting

492 at these sites is close to the critical point of seawater. Very high REE concentrations may
493 reflect the dramatic increase in stability of chloride complexes as fluids approach a
494 supercritical state (Ding and Seyfried, 1992; Shmulovich *et al*., 2002), and the enhanced
495 capacity of the vapour-phase fluid for metal dissolution by ion hydration (Pokrovski *et al*.,
496 2005). Sulphate also forms strong complexes with the REEs at high temperatures, and
497 stability constants with SO_4^{2-} are highest for the MREE (Schijf and Byrne, 2004). However,
498 as complexes with chloride are strongest for the LREEs, and the availability of free sulphate
499 ions is substantially reduced at such high temperatures, complexation effects are unlikely to
500 generate the observed REE fractionation in fluids at Black & White and Two Boats (Schmidt
501 *et al*., 2010). Model simulations indicate that vapour-phase fluids mix continuously with
502 conductively heated seawater in the shallow subsurface, which facilitates precipitation of
503 anhydrite (Coumou *et al*., 2009). Consequently, we suggest that entrainment of anhydrite
504 into fluids may be characteristic of fluids close to the critical point of seawater, resulting in
505 high REE concentrations. Assimilation of the REEs into anhydrite is controlled by a
506 combination of crystal lattice constraints and fluid speciation, as discussed in Section 5.5.
507 Hydrothermal anhydrite recovered from the chimney of Black & White is enriched in the
508 MREE (Figure 3), which likely overprints a more 'typical' REE distribution pattern in fluids,
509 consistent with observations at Two Boats.

510 The large ionic radius of divalent europium inhibits its partitioning into anhydrite, and
511 the magnitude of the Eu anomaly in the remaining fluid is thought to be a proxy for the
512 degree of fluid evolution in mid-ocean ridge systems (Humphris, 1998; Schmidt *et al.*, 2010).
513 Figure 8 indicates that there is an inverse relationship between the size of the Eu anomaly and
514 the total REE concentration in endmember fluids from the ESR. Fluids from Black & White
515 (E9 North) have high ∑REE and a negative Eu anomaly, which may be indicative of an early
516 evolutionary stage, prior to significant anhydrite deposition (Schmidt *et al.*, 2010). This is

517 also suggested as an alternative explanation for the REE_{CN} distribution pattern reported for
518 Two Boats by Schmidt *et al*. (2010). In this connection, the water-rock ratio in the reaction
519 zone at Black & White is ~2 times higher than those estimated for the other E9 vent sites (and
520 ~4 times higher than estimated for E2 sites) (James *et al*., in review). This indicates that the
521 extent of water-rock interaction is more limited, so REE concentrations are less extensively
522 modified by alteration reactions, complexation and/or sorption effects (Shibata *et al*., 2006;
523 Schmidt *et al*., 2010). Moreover, it has been suggested that the composition of hydrothermal
524 fluids is significantly modified during transport from the reaction zone to the seafloor (Bach
525 and Irber, 1998). These authors suggest that fluids in the reaction zone have high ΣREE,
526 relatively flat REE_{CN} distribution patterns, and a negative Eu anomaly. During ascent to the
527 seafloor, REE concentrations are modified by complexation with chloride and other aqueous
528 ligands, exchange reactions and mineral precipitation, resulting in a LREE-enriched fluid
529 with a positive Eu anomaly. Thus, the Black & White (and Two Boats) fluids may represent
530 rarely sampled, primary reaction-zone fluids. By contrast, fluids from E9 South have low
531 ∑REE but large positive Eu anomalies which point to extensive subsurface anhydrite
532 deposition, potentially augmented by more extensive water-rock reactions, and strong Eu-Cl
533 complexation.

534

535 **5.5 Anhydrite as a Recorder of Past Vent Fluid Compositions**

536 The distribution pattern of the REEs in anhydrites recovered from white smoker
537 chimneys at Winter Palace in the Kemp Caldera is very different from that of the vent fluids
538 being expelled today. The anhydrites are remarkably enriched in the HREEs (La_{CN}/Yb_{CN} =
539 0.03 – 0.09; Table 4), whereas the vent fluids have relatively flat REE_{CN} patterns, with
540 La_{CN}/Yb_{CN} = 2.1 – 2.2. Thus, either the REEs are strongly fractionated during anhydrite

deposition, or the anhydrite precipitated from a fluid that had a different composition from the fluids venting at this site today.

Rare earth elements are incorporated into the $CaSO_4$ lattice by substitution of Ca^{2+}, so crystallographic constraints dictate that ion exchange will favour those REEs with an ionic radius similar to calcium (Morgan and Wandless, 1980). Experimentally determined partition coefficients (K_D) for the REEs in solution and anhydrite are highest for Ce^{3+}, Nd^{3+}, and Sm^{3+}, so the MREEs should be preferentially incorporated into anhydrite (Kagi *et al.*, 1993; Schmidt *et al.*, 2010). However, REE distribution patterns in anhydrite recovered from the TAG hydrothermal site on the Mid-Atlantic Ridge, normalised to the vent fluids, are variable (Humphris, 1998), and K_D values for La, Ce and Nd are anomalously low (Mills and Elderfield, 1995). It has therefore been suggested that uptake of the REEs into anhydrite is principally controlled by fluid composition, because of the effects of complexation on the availability of free ions in fluids (Humphris and Bach, 2005). In support of this, variable REE distribution patterns in anhydrites from PACMANUS (including enrichments in the middle- and heavy-REEs) are considered to reflect variations in the concentration of magmatic volatiles in the vent fluids from which they precipitated (Craddock and Bach, 2010).

As the anhydrites sampled from Kemp Caldera are strongly enriched in the HREEs (Figures 3 and 4), REE uptake cannot be primarily controlled by crystallographic constraints. By contrast, if the REE composition of the anhydrite reflects that of the fluid, then the composition of the vent fluids must have been different at the time the anhydrite was deposited. According to Craddock *et al*. (2010), heavy-REE enrichments are favoured in hydrothermal fluids with high fluoride concentrations, and high F^-/Cl^- ratios, whereas enrichment of all REEs (and relatively flat REE_{CN} patterns, as observed in Kemp Caldera fluids today) is due to very low fluid pH.

As discussed in Section 2.2, the floor of the Kemp Caldera is covered in ash and sulphur deposits, which suggests that there has been a magmatic blow out event at this site in the recent past. Such a surge in magmatic activity would enhance the supply of REE-binding ligands, including F^-, and high temperatures would promote phase separation which would increase the F^-/Cl^- ratio of the vent fluids, enhancing the mobilisation of the HREEs in particular (Wood, 1990). As the extent of water-rock interaction is likely to have been reduced during a burst of magmatic activity, SO_2 disproportionation in the subsurface may have been limited, and fluid pH would be higher than it is today (1 ± 1; Section 2.2). Consequently, a strong efflux of magmatic HF would provide free F^- for complexation, enhancing the concentration of HREE in fluids for incorporation into anhydrite. By contrast, the low pH of the fluids venting today results in non-selective REE mobilisation and limits the availability of fluoride as a complexing ligand, producing flat REE distribution patterns.

6. SUMMARY AND CONCLUSIONS

Rare earth element data are reported for a suite of high-temperature and diffuse hydrothermal fluids, and conjugate chimney anhydrite, for newly-discovered vent sites in the East Scotia Sea subduction zone system. High temperature fluids from E2 and E9 South are enriched in the light REEs and have positive Eu anomalies, like most vent fluids from basalt-hosted mid-ocean ridge spreading centres. This REE_{CN} pattern is best described in terms of differential leaching of the REEs from alteration minerals in the host rock, and stabilisation of the REEs as chloride complexes. The fluids appear to be unaffected by inputs of material from the nearby subduction zone. By contrast, fluids from E9 North are enriched in the middle REEs and have negative Eu anomalies, whereas fluids from Kemp Caldera have flat chondrite-normalised REE patterns. Fluids from E9 North appear to be affected by dissolution of anhydrite, which has high ∑REE and a negative Eu anomaly. Alternatively,

591 the extent of water-rock interaction at E9 North may be limited, resulting in a relatively un-
592 evolved REE pattern. At Kemp Caldera, REE solubility in the fluids venting at the present-
593 day appears to be critically dependent on very low pH.

594 The REE_{CN} patterns of chimney anhydrites from E2 and E9 are similar to their
595 conjugate high temperature fluids, but anhydrite recovered from the Winter Palace site at
596 Kemp Caldera is strongly enriched in the heavy REEs relative to the present-day vent fluids.
597 We suggest that these anhydrites precipitated from fluids that were strongly enriched in HF,
598 probably introduced during a relatively recent magmatic blow-out event.

599 This study indicates that the REE composition of hydrothermal fluids can provide
600 critical information about sub-seafloor geochemical processes associated with hydrothermal
601 activity in subduction zone settings. These include reactions between host rock and
602 circulating fluids, phase separation and fluid evolution, magmatic acid volatile degassing, and
603 mineral precipitation. We have also shown that analysis of the REE composition of
604 associated anhydrite deposits can provide insight as to the nature of hydrothermal activity in
605 the past, where access to hydrothermal fluids is precluded.

606

607 **ACKNOWLEDGMENTS**

608 We would like to thank the Captain and crew of the *RRS James Cook* and the *ROV ISIS*
609 technical team on cruise JC42 for facilitating the collection of our samples. We thank: Dr
610 Andy Milton and Dr Matt Cooper for assistance with REE and Sr isotope measurements at
611 Southampton; Prof. Martin Frank and group at GEOMAR, Kiel, for the seaFAST analyses;
612 Darryl Green and Belinda Alker for both ship-board and onshore laboratory assistance; and
613 Ross Williams for XRD analyses. This work was funded by Natural Environment Research

614 Council (NERC) consortium grant NE/D01249X/1, NERC National Capability, and the
615 Graduate School of the National Oceanography Centre, Southampton.

616

617 **REFERENCES**

618

619 Aiuppa A., Baker D. R. and Webster J. D. (2009) Halogens in volcanic systems. *Chem. Geol.*
620 **263,** 1-18.

621 Allen D. E. and Seyfried Jr W. E. (2005) REE controls in ultramafic hosted MOR
622 hydrothermal systems: An experimental study at elevated temperature and pressure.
623 *Geochim. Cosmochim. Acta* **69,** 675-683.

624 Auzende J.-M., Ballu V., Batiza R., Bideau D., Charlou J. L., Cormier M. H., Fouquet Y.,
625 Geistdoerfer P., Lagabrielle Y., Sinton J. and Spadea P. (1996) Recent tectonic,
626 magmatic, and hydrothermal activity on the East Pacific Rise between 17°S and 19°S:
627 Submersible observations. *J. Geophys. Res.* **101,** 17995-18010.

628 Bach W. and Irber W. (1998) Rare earth element mobility in the oceanic lower sheeted dyke
629 complex: evidence from geochemical data and leaching experiments. *Chem. Geol*.
630 **151**, 309-326.

631 Bach W., Roberts S., Vanko D. A., Binns R. A., Yeats C. J., Craddock P. R. and Humphris S.
632 E. (2003) Controls of fluid chemistry and complexation on rare-earth element
633 contents of anhydrite from the Pacmanus subseafloor hydrothermal system, Manus
634 Basin, Papua New Guinea. *Miner. Deposita* **38,** 916-935.

635 Bach W., Roberts S. and Binns R. A. (2005) Data Report: Chemical and Isotopic (S, Sr)
636 Composition of Anhydrite from ODP Leg 193, PACMANUS Hydrothermal System,
637 Manus Basin, Papua New Guinea. *In:* Barriga F. J. A. S., Binns R. A., Miller D. J.
638 and Herzig P. (eds.) *Proceedings of the Ocean Drilling Program, Scientific Results.*
639 pp. 1-23

640 Bai T. B. and Koster van Groos A. F. (1999) The distribution of Na, K, Rb, Sr, Al, Ge, Cu,
641 W, Mo, L, and Ce between granitic melts and coexisting aqueous fluids. *Geochim.*
642 *Cosmochim. Acta* **63,** 1117-1131.

643 Barker P. F. (1970) Plate tectonics of the Scotia Sea Region. *Nature* **228,** 1293-1296.

644 Bau M. (1991) Rare-earth element mobility during hydrothermal and metamorphic fluid-rock
645 interaction and the significance of the oxidation state of europium. *Chem. Geol.* **93,**
646 219-230.

647 Bau M. and Dulski P. (1999) Comparing yttrium and rare earths in hydrothermal fluids from
648 the Mid-Atlantic Ridge: implications for Y and REE behaviour during near-vent
649 mixing and for the Y/Ho ratio of Proterozoic seawater. *Chem. Geol.* **155,** 77-90.

650 Bischoff J. L. and Rosenbauer R. J. (1984) The critical point and two-phase boundary of
651 seawater, 200 - 500 ˚C. *Earth Planet. Sci. Lett.* **68,** 172-180.

652 Brett C. P. (1977) Seismicity of the South Sandwich Islands region. *Geophys. J. Roy. Astr. S.*
653 **51,** 453-464.

654 Bruguier N. J. and Livermore R. A. (2001) Enhanced magma supply at the southern East
655 Scotia Ridge: evidence for mantle flow around the subducting slab? *Earth Planet. Sci.*
656 *Lett.* **191,** 129-144.

657 Butterfield D., Massoth G. J., McDuff R. E., Lupton J. and Lilley M. D. (1990) Geochemistry
658 of hydrothermal fluids from Axial Seamount Hydrothermal Emissions Study Vent
659 Field, Juan de Fuca Ridge: Subseafloor boiling and subsequent fluid-rock interaction.
660 *J. Geophys. Res.* **95,** 12895-12921.

661 Campbell A. C., Bowers T. S., Measures C. I., Falkner K. K., Khadem M. and Edmond J. M.
662 (1988) A time series of vent fluid compositions from 21°N, East Pacific Rise (1979,
663 1981, 1985), and the Guaymas Basin, Gulf of California (1982, 1985). *J. Geophys.*
664 *Res.* **93,** 4537-4549.

665 Charlou J. L., Fouquet Y., Donval J. P. and Auzende J.-M. (1996) Mineral and gas chemistry
666 of hydrothermal fluids on an ultrafast spreading ridge: East Pacific Rise, 17° to 19°S
667 (Naudur cruise, 1993). Phase separation processes controlled by volcanic and
668 tectonic activity. *J. Geophys. Res.* **101,** 15899-15919.

669 Coumou D., Driesner T., Weis P. and Heinrich C. A. (2009). Phase separation, brine
670 formation, and salinity variation at Black Smoker hydrothermal systems. *J. Geophys.*
671 *Res.*, **114**, 10.1029/2008jb005764

672 Craddock P. R. and Bach W. (2010) Insights to magmatic–hydrothermal processes in the
673 Manus back-arc basin as recorded by anhydrite. *Geochim. Cosmochim. Acta* **74,**
674 5514-5536.

675 Craddock P. R., Bach W., Seewald J. S., Rouxel O. J., Reeves E. and Tivey M. K. (2010)
676 Rare earth element abundances in hydrothermal fluids from the Manus Basin, Papua
677 New Guinea: Indicators of sub-seafloor hydrothermal processes in back-arc basins.
678 *Geochim. Cosmochim. Acta* **74,** 5494-5513.

679 de Ronde C. E. J., Massoth G. J., Butterfield D. A., Christenson B. W., Ishibashi J.,
680 Ditchburn R. G., Hannington M. D., Brathwaite R. L., Lupton J. E., Kamenetsky V.
681 S., Graham I. J., Zellmer G. F., Dziak R. P., Embley R. W., Dekov V. M., Munnik F.,
682 Lahr J., Evans L. J. and Takai K. (2011) Submarine hydrothermal activity and gold-
683 rich mineralization at Brothers Volcano, Kermadec Arc, New Zealand. *Miner.*
684 *Deposita* **46**, 541-584.

685 Ding K. and Seyfried W. E. (1992) Determination of Fe-Cl complexing in the low-pressue
686 supercritical region (NaCl fluid) – iron solubility constraints on pH of subseafloor
687 hydrothermal fluids. *Geochim. Cosmochim. Acta* **56**, 3681-3692.

688 Douville E., Bienvenu P., Charlou J. L., Donval J. P., Fouquet Y., Appriou P. and Gamo T.
689 (1999) Yttrium and rare earth elements in fluids from various deep-sea hydrothermal
690 systems. *Geochim. Cosmochim. Acta* **63,** 527-643.

691 Douville E., Charlou J. L., Oelkers E. H., Bienvenu P., Jove Colon C. F., Donval J. P.,
692 Fouquet Y., Prieur D. and Appriou P. (2002) The Rainbow vent fluids (36° 14'N,
693 MAR): the influence of ultramafic rocks and phase separation on trace metal content
694 in Mid-Atlantic Ridge hydrothermal fluids. *Chem. Geol.* **184,** 37-48.

695 Edmond J. M., Measures C. I., McDuff R. E., Chan L. H., Collier R., Grant B., Gordon L. I.
696 and Corliss J. B. (1979) Ridge crest hydrothermal activity and the balances of the
697 major and minor elements in the Ocean: The Galapagos data. *Earth Planet. Sci. Lett.*
698 **46,** 1-18.

699 Elderfield H., Whitfield M., Burton J. D., Bacon M. P. and Liss P. S. (1988) The oceanic
700 chemistry of the rare earth elements. *Phil. Trans. R. Soc. A* **325,** 105-126.

701 Embley R. W., Baker E. T., Butterfield D. A., Chadwick W. W., Lupton J. E., Resing J. A.,
702 de Ronde C. E. J., Nakamura K.-i., Tunnicliffe V., Dower J. F. and Merle S. G.
703 (2007) Exploring the submarine ring of fire. Mariana Arc to Western Pacific.
704 *Oceanography* **20,** 68-79.

705 Fouquet Y., von Stackelberg U., Charlou J. L., Donval J. P., Foucher J. P., Erzinger J., Herzig
706 P., Mühe R., Wiedicke M., Soakai S. and Whitechurch H. (1991) Hydrothermal
707 activity in the Lau back-arc basin: Sulfides and water chemistry. *Geology* **19,** 303.

708 Fretzdorff S., Livermore R. A., Devey C. W., Leat P. T. and Stoffers P. (2002) Petrogenesis
709 of the Back-arc East Scotia Ridge, South Atlantic Ocean. *J. Petrol.* **43,** 1435-1467.

710 Gammons C. H., Wood S. A. and Williams-Jones A. E. (1996) The aqueous geochemistry of
711 the rare earth elements and yttrium: VI. Stability of neodymium chloride complexes
712 from 25 to 300°C. *Geochim. Cosmochim. Acta* **60,** 4615-4630.

713 Gamo T., Chiba H., Masuda H., Edmonds H. N., Fujioka K., Kodama Y., Nanba H. and Sano
714 Y. (1996) Chemical characteristics of hydrothermal fluids from the TAG mound of
715 the mid-Atlantic Ridge in August 1994: implications for spatial and temporal
716 variability of hydrothermal activity. *Geophys. Res. Lett.* **23,** 3483-3486.

717 Gamo T., Okamura K., Charlou J.-L., Urabe T., Auzende J.-M., Ishibashi J., Shitashima K.,
718 Chiba H. and Shipboard Scientific Party of the ManusFlux C. (1997) Acidic and
719 sulfate-rich hydrothermal fluids from the Manus back-arc basin, Papua New Guinea.
720 *Geology* **25,** 139-142.

721 German C. R., Klinkhammer G. P., Edmond J. M., Mitra A. and Elderfield H. (1990)
722 Hydrothermal scavenging of rare-earth elements in the ocean. *Nature* **345,** 516-518.

723 German C. R., Livermore R. A., Baker E. T., Bruguier N. I., Connelly D. P., Cunningham A.
724 P., Morris P., Rouse I. P., Statham P. J. and Tyler P. A. (2000) Hydrothermal plumes
725 above the East Scotia Ridge: an isolated high-latitude back-arc spreading centre.
726 *Earth Planet. Sci. Lett.* **184,** 241-250.

727 Haas J. R., Shock E. L. and Sassani D. C. (1995) Rare earth elements in hydrothermal
728 systems: Estimates of standard partial molal thermodynamic properties of aqueous

729 complexes of the rare earth elements at high pressures and temperatures. *Geochim.*
730 *Cosmochim. Acta* **59,** 4329-4350.

731 Hathorne E. C., Haley B., Stichel T., Grasse P., Zieringer M. and Frank M. (2012). Online
732 preconcentration ICP-MS analysis of rare earth elements in seawater. *Geochem.*
733 *Geophys. Geosys.*, **13**, 10.1029/2011GC003907

734 Humphris S. (1998). Rare earth element composition of anhydrite: Implications for
735 deposition and mobility within the active TAG hydrothermal mound. *In:* Herzig P.,
736 Humphris S., Miller D. J. and Zierenberg R. A. (eds.) *Proceedings of the Ocean*
737 *Drilling Program, Scientific Results.* pp. 143-159

738 Humphris S. and Bach W. (2005) On the Sr isotope and REE compositions of anhydrites
739 from the TAG seafloor hydrothermal system. *Geochim. Cosmochim. Acta* **69,** 1511-
740 1525.

741 Iwasaki I. and Ozawa T. (1960) Genesis of sulfate in acid hot spring. *B. Chem. Soc. Jpn.* **33,**
742 1018-1019.

743 James R. H., Elderfield H. and Palmer M. R. (1995) The chemistry of hydrothermal fluids
744 from the Broken Spur site, 29ºN Mid-Atlantic Ridge. *Geochim. Cosmochim. Acta* **59**,
745 651-659.

746 James R. H., Green D. R. H., Stock M. J., Alker B. J., Banerjee N. R., Cole C., German C. R.,
747 Huvenne V. A. I., Powell A. M. and Connelly D. P. (in review, *Geochim. Cosmochim.*
748 *Acta*) Geochemistry of hydrothermal fluids and associated mineralisation on the East
749 Scotia Ridge.

750 Kagi H., Dohmoto Y., Takano S. and Masuda A. (1993) Tetrad effect in lanthanide
751 partitioning between calcium sulfate crystal and its saturated solution. *Chem. Geol.*
752 **107,** 71-82.

753 Kelley D. S., Baross J. A. and Delaney J. R. (2002) Volcanoes, fluids, and life at mid-ocean
754 ridge spreading centers. *Annu. Rev. Earth Planet. Sci.* **30,** 385-491.

Klinkhammer G. P., Elderfield H., Edmond J. M. and Mitra A. (1994) Geochemical implications of rare earth element patterns in hydrothermal fluids from mid-ocean ridges. *Geochim. Cosmochim. Acta* **58,** 5105-5113.

Larter R., Vanneste L., Morris P. and Smythe D. K. (2003). Structure and tectonic evolution of the South Sandwich arc. *In:* Larter R. and Leat P. T. (eds.) *Intra-Oceanic Subduction Systems: Tectonic and Magmatic Processes.* London: The Geological Society of London, pp. 255-284

Leat P. T., Livermore R. A., Millar I. L. and Pearce J. A. (2000) Magma supply in back-arc spreading centre segment E2, East Scotia Ridge. *J. Petrol.* **41,** 845-866.

Leat P. T., Pearce J. A., Barker P. F., Millar I. L., Barry T. L. and Larter R. D. (2004) Magma genesis and mantle flow at a subducting slab edge: the South Sandwich arc-basin system. *Earth Planet. Sci. Lett.* **227,** 17-35.

Leybourne M. I., Schwarz-Schampera U., de Ronde C. E. J., Baker E. T., Faure K., Walker S. L., Butterfield D. A., Resing J. A., Lupton J. E., Hannington M. D., Gibson, H. L., Massoth G. J., Embley R. W., Chadwick Jr W. W., Clark M. R., Timm C., Graham I. J. And Wright I. C. (2012) Submarine magmatic-hydrothermal systems at the Monowai Volcanic Center, Kermadec Arc. *Econ. Geol*. **107**, 1669-1694.

Livermore R. A., McAdoo D. and Marks K. (1994) Scotia Sea tectonics from high-resolution satellite gravity. *Earth Planet. Sci. Lett.* **123,** 255-268.

Livermore R. A., Cunningham A., Vanneste L. and Larter R. (1997) Subduction influence on magma supply at the East Scotia Ridge. *Earth Planet. Sci. Lett.* **150,** 261-275.

Michard A., Albarède F., Michard G., Minster J. F. and Charlou J. L. (1983) Rare-earth elements and uranium in high temperature solutions from the East Pacific Rise hydrothermal vent field (13°N). *Nature* **303,** 795-897.

Michard A. and Albarède F. (1986) The REE content of some hydrothermal fluids. *Chem. Geol.* **55,** 51-60.

Migdisov A. A., Williams-Jones A. E. and Wagner T. (2009) An experimental study of the solubility and speciation of the Rare Earth Elements (III) in fluoride- and chloride-

783 bearing aqueous solutions at temperatures up to 300°C. *Geochim. Cosmochim. Acta*
784 **73,** 7087-7109.

785 Mills R. and Elderfield H. (1995) Rare earth element geochemistry of hydrothermal deposits
786 from the active TAG mound, 26°N Mid-Atlantic Ridge. *Geochim. Cosmochim. Acta*
787 **59,** 3511-3524.

788 Mitra A., Elderfield H. and Greaves M. J. (1994) Rare earth elements in submarine
789 hydrothermal fluids and plumes from the Mid-Atlantic Ridge. *Mar. Chem.* **46,** 217-
790 235.

791 Morgan J. W. and Wandless G. A. (1980) Rare earth element distribution in some
792 hydrothermal minerals: Evidence for crystallographic control. *Geochim. Cosmochim.*
793 *Acta* **44,** 973-980.

794 Mottl M. J., Seewald J. S., Wheat C. G., Tivey M. K., Michael P. J., Proskurowski G.,
795 McCollom T. M., Reeves E., Sharkey J., You C. F., Chan L. H. and Pichler T. (2011)
796 Chemistry of hot springs along the Eastern Lau Spreading Center. *Geochim.*
797 *Cosmochim. Acta* **75,** 1013-1038.

798 Palmer M. (1992) Controls over the chloride concentration of submarine hydrothermal vent
799 fluids - evidence from Sr/Ca and Sr-87/Sr-86 ratios. *Earth Planet. Sci. Lett.* **109,** 37-
800 46.

801 Pelayo A. M. and Wiens D. A. (1989) Seismotectonics and relative plate motions in the
802 Scotia Sea region. *J. Geophys. Res.* **94,** 7293-7320.

803 Phinney W. C. and Morrison D. A. (1990) Partition coefficients for calcic plagioclase:
804 Implications for Archean anorthosites. *Geochim. Cosmochim. Acta* **54,** 1639-1654.

805 Pokrovski G. S., Roux J. and Harrichoury J-C. (2005) Fluid density control on vapour-liquid
806 partitioning of metals in hydrothermal systems. *Geology* **33**, 657-660.

807 Powell A. P., Banerjee N. R., Munro L. E., Hisao G. and James R. H. (2011) Investigations
808 of deep-sea hydrothermal samples for isotopic composition and interfering
809 compounds using CRDS. *IAEA International Symposium on Stable Isotopes in*

Hydrology, Marine Ecosystems and Climate chnge Studies, Oceanographic Museum of Monaco, 27 March – 1 April 2011.

Reeves E. P., Seewald J. S., Saccocia P., Bach W., Craddock P. R., Shanks W. C., Sylva S. P., Walsh E., Pichler T. and Rosner M. (2011) Geochemistry of hydrothermal fluids from the PACMANUS, Northeast Pual and Vienna Woods hydrothermal fields, Manus Basin, Papua New Guinea. *Geochim. Cosmochim. Acta* **75,** 1088-1123.

Rogers A. D., Tyler P. A., Connelly D. P., Copley J. T., James R., Larter R. D., Linse K., Mills R. A., Garabato A. N., Pancost R. D., Pearce D. A., Polunin N. V. C., German C. R., Shank T., Boersch-Supan P. H., Alker B. J., Aquilina A., Bennett S. A., Clarke A., Dinley R. J. J., Graham A. G. C., Green D. R. H., Hawkes J. A., Hepburn L., Hilario A., Huvenne V. A. I., Marsh L., Ramirez-Llodra E., Reid W. D. K., Roterman C. N., Sweeting C. J., Thatje S. and Zwirglmaier K. (2012). The discovery of new deep-sea hydrothermal vent communities in the Southern Ocean and implications for biogeography. *PLoS Biol.*, **10**, 10.1371/journal.pbio.1001234

Schijf J. and Byrne R. H. (2004) Determination of $SO_4\beta_1$ for yttrium and the rare earth elements at I = 0.66 m and t = 25°C – Implications for YREE solution speciation in sulfate-rich waters. *Geochim. Cosmochim. Acta* **68**, 2825-2837.

Schmidt K., Garbe-Schönberg D., Bau M. and Koschinsky A. (2010) Rare earth element distribution in >400°C hot hydrothermal fluids from 5°S, MAR: The role of anhydrite in controlling highly variable distribution patterns. *Geochim. Cosmochim. Acta* **74,** 4058-4077.

Seyfried Jr W. E. and Ding K. (1995) The hydrothermal chemisty of fluoride in seawater. *Geochim. Cosmochim. Acta* **59,** 1063-1071.

Shannon R. D. (1976) Revised effective ionic radii and systematic studies of interatomic distances in halides and chalcogenides. *Acta Crystallogr.* **32,** 751-767.

Sherrell R. M., Field M. P. and Ravizza G. (1999) Uptake and fractionation of rare earth elements on hydrothermal plume particles at 9° 45'N, East Pacific Rise. *Geochim. Cosmochim. Acta* **63,** 1709-1722.

838 Shibata S.-N., Tanaka T. and Yamamoto K. (2006) Crystal structure control of the dissolution
839 of rare earth elements in water-mineral interactions. *Geochem. J.* **40**, 437-446.

840 Shmulovich K., Heinrich W., Möller P. and Dulski P. (2002) Experimental determination of
841 REE fractionation between liquid and vapour in the systems NaCl-H_2O and $CaCl_2$-
842 H_2O up to 450 °C. *Contrib. Mineral. Petrol.* **44**, 257-273.

843 Stichel T., Frank M., Rickli J. and Haley B. A. (2012) The hafnium and neodymium isotope
844 composition of seawater in the Atlantic sector of the Southern Ocean. *Earth Planet.*
845 *Sci. Lett.* **317-318,** 282-294.

846 Taylor S. R. and McClennan S. M. (1985) *The Continental Crust: Its Composition and*
847 *Evolution,* Oxford, UK, Blackwell Scientific Publications.

848 Thomas C., Livermore R. A. and Pollitz F. (2003) Motion of the Scotia Sea plates. *Geophys.*
849 *J. Int.* **155,** 789-804.

850 van de Flierdt T., Pahnke K., Amakawa H., Andersson P., Basak C., Coles B., Colin C.,
851 Crocket K., Frank M. and Frank N. (2012) GEOTRACES intercalibration of
852 neodymium isotopes and rare earth element concentrations in seawater and suspended
853 particles. Part 1: reproducibility of results for the international intercomparison.
854 *Limnol. Oceanogr. Methods* **10,** 234-251.

855 Van Dover C. L. (2000) *The Ecology of Deep Sea Hydrothermal Vents*, Princeton University
856 Press.

857 Von Damm K. L., Edmond J. M., Grant B., Measures C. I., Walden B. and Weiss R. F.
858 (1985) Chemistry of submarine hydrothermal solutions at 21°N, East Pacific Rise.
859 *Geochim. Cosmochim. Acta* **49,** 2197-2220.

860 Von Damm K. L. and Bischoff J. L. (1987) Chemistry of hydrothermal solutions from the
861 southern Juan de Fuca Ridge. *J. Geophys. Res.* **92,** 11334-11346.

862 Von Damm K. L. (1990) Seafloor hydrothermal activity: black smoker chemistry and
863 chimneys. *Annu. Rev. Earth Planet. Sci.* **18,** 173-204.

864 Williams-Jones A. E., Migdisov A. A. and Samson I. M. (2012) Hydrothermal mobilisation
865 of the rare earth elements - a tale of "ceria" and "yttria". *Elements* **8,** 355-360.

866 Wood S. A. (1990) The aqueous geochemistry of the rare-earth elements and yttrium. 2.
867 Theoretical predictions of speciation in hydrothermal solutions to 350°C at saturation
868 water vapour pressure. *Chem. Geol.* **88,** 99-125.

Table 1. Total REE concentrations and $^{87}Sr/^{86}Sr$ ratios of sampled (*s.*) and end-member (EM) hydrothermal fluids from the East Scotia Ridge and Kemp Caldera.

			T_{max} °C	Mg mmol/kg	La	Ce	Pr	Nd	Sm	Eu	Gd	Tb	Dy	Ho	Er	Tm	Yb	Lu	∑REE *nmol/kg*	$^{87}Sr/^{86}Sr$
E2																				
Dog's Head	130-B2-08	***s.***	323	2.28	8060	17,400	2200	9140	2060	1880	1900	233	1100	175	370	37	190	23	45	0.704355
	130-B2-05	***s.***	323	2.11	8670	16,000	2000	8120	1800	2290	1800	201	955	155	321	34	175	21	42	0.704352
	132-Y1-07	***s.***	351	1.02	6280	11,600	1360	5260	1060	1270	1000	117	566	94	215	23	130	16	29	0.704241
		EM	**351**	**0**	**7920**	**15,500**	**1900**	**7750**	**1700**	**1870**	**1610**	**190**	**902**	**146**	**311**	**32**	**170**	**21**	**40**	**0.704168**
Sepia	135-B2-08	***s.***	347	1.61	6580	11,900	1340	5100	976	1210	960	111	533	88	191	20	119	15	29	0.704171
		EM	**353**	**0**	**6790**	**12,200**	**1380**	**5250**	**1010**	**1250**	**986**	**114**	**549**	**91**	**197**	**21**	**123**	**16**	**30**	**0.704035**
E9 North																				
Black & White	140-Y2-04	***s.***	380	0.58	9660	32,900	5740	30,100	7980	1450	7300	934	4320	643	1250	101	452	46	103	0.706029
	142-Y2-01	***s.***	383	8.35	12,600	41,200	6880	36,500	9480	1890	9700	1120	5010	749	1420	120	483	53	127	0.707598
		EM	**383**	**0**	**11,900**	**39,700**	**6780**	**35,700**	**9380**	**1790**	**9060**	**1100**	**5020**	**748**	**1430**	**119**	**504**	**53**	**123**	**0.705762**
E9 South																				
Ivory Tower	142-B2-05	***s.***	348	1.96	1220	2480	306	1220	248	1090	220	24	121	23	52	5.8	39	5.2	7	0.705152
		EM	**348**	**0**	**1260**	**2580**	**317**	**1270**	**257**	**1130**	**223**	**25**	**125**	**24**	**54**	**6.0**	**40**	**5.3**	**7.3**	**0.704610**
Launch Pad	144-B1-02	***s.***	351	4.45	1010	1800	217	873	178	3250	150	18	89	18	37	5.2	26	4.2	7.7	0.706177
	144-B1-03	***s.***	351	12.9	770	1360	167	671	140	2480	120	13	69	12	28	3.4	20	2.4	5.9	0.707408
		EM	**351**	**0**	**1060**	**1890**	**229**	**921**	**189**	**3440**	**161**	**18**	**93**	**17**	**38**	**5.0**	**26**	**3.8**	**8.1**	**0.705014**
Pagoda	144-Y1-06	***s.***	351	0.84	1129	2050	253	1050	223	3280	200	27	147	27	77	8.7	53	7.1	8.5	0.705121
	144-Y1-07	***s.***	351	2.34	981	1700	207	844	184	3160	1200	19	95	18	33	4.2	24	3.2	7.4	0.705456
		EM	**351**	**0**	**1090**	**1930**	**237**	**978**	**210**	**3320**	**187**	**24**	**125**	**23**	**57**	**6.7**	**40**	**5.3**	**8.2**	**0.704890**
Kemp Caldera																				
Great Wall	147-Y2-04	***s.***	21	50.1	543	1070	155	783	208	97	280	41	260	56	163	22	136	22	3.8	n/a
Winter Palace	149-B1-02	***s.***	n/a	43.0	189	368	54	222	56	55	100	18	109	21	58	7.9	49	7.6	1.3	0.708883
	152-Y2-01	***s.***	23	51.7	64	46	11	47	10	4.0	16	3.3	26	6.1	18	2.7	16	2.5	0.3	0.709142
	152-Y1-06	***s.***	28	48.4	118	185	36	166	50	19	73	15	109	25	77	12	85	14	1.0	0.708998
Seawater			0	53	42	6.2	6.3	27	5.0	1.2	6.8	1.0	7.7	2.1	7.2	1.1	7.7	1.4	0.1	0.709182

s. = sampled fluids; EM = endmember fluids; T_{max} = highest measured fluid temperature; n/a = not available; concentrations in pmol/kg unless otherwise stated; seawater is Southern Ocean Circumpolar Deep Water (ts PS71 131-1) analysed in this study.

Table 2. Temperature, [Cl], [Mg], [SO_4] and chondrite-normalised REE ratios of endmember fluids from the East Scotia Ridge and sampled fluids from Kemp Caldera, as well as other representative hydrothermal vent sites. The ratios La_{CN}/Yb_{CN}, La_{CN}/Nd_{CN}, and Nd_{CN}/Yb_{CN} allow comparison of, respectively, light to heavy (LREE/HREE), light to mid (LREE/MREE) and mid to heavy (MREE/HREE) REE abundance. The europium anomaly, (Eu_{CN}/Eu^*_{CN}), where Eu* represents the averaged concentration of neighbouring REEs, Sm and Gd, is also given.

	T_{max} °C	[Cl^-] mM	[Mg] mM	∑REE nM	La_{CN}/Yb_{CN}	La_{CN}/Nd_{CN}	Nd_{CN}/Yb_{CN}	Eu_{CN}/Eu^*_{CN}	[SO_4^{2-}] mM
East Scotia Ridge									
E2									
Dog's Head	351	536	0	40.0	25.2	1.87	13.5	3.45	1.31
Sepia	353	532	0	30.0	30.0	2.37	12.7	3.84	0.97
E9 North									
Black & White	383	98.2	0	123	12.8	0.61	21.0	0.59	3.57
E9 South									
Ivory Towers	348	220	0	7.3	17.2	1.82	9.47	14.3	0.26
Launch Pad	351	179	0	8.1	21.8	2.11	10.3	59.5	< 0
Pagoda	351	220	0	8.2	14.9	2.04	7.33	50.9	0.96
Kemp Caldera									
Great Wall	21	511	50	3.8	2.16	1.27	1.70	1.23	25.6
Winter Palace	(212)	462	43	1.32	2.09	1.56	1.34	2.22	21.6
Mid-Atlantic Ridge									
TAG, 26 °N[Ŧ]	363	638	0	23.8	11.4	2.06	5.52	9.25	<0.2
Lucky Strike, 37 °N[Ŧ]	324	413	0	19.3	37.1	3.16	11.7	4.65	<0.2
Two Boats, 5 °S[λ]	412	298	0	104	5.79	0.80	7.23	0.56	-
East Pacific Rise									
Elsa, 13 °N[Ŧ]	340	723	0	45.3	14.8	1.78	8.30	7.94	<0.2
Nadir, 17-19 °S[Ŧ]	340	190	0	6.08	28.4	2.73	10.4	39.8	<0.2
Lau Basin									
Vai Lili[Ŧ]	334	667	0	62.6	32.6	3.25	10.0	12.3	<0.2
Manus Basin									
Snowcap SC2[φ]	180	-	24.2	1.96	4.77	2.27	2.10	8.03	-
Snowcap SC1[φ]	152	-	30.8	1.40	1.71	2.30	0.74	4.47	-
DESMOS D1[φ]	117	492	46.0	147	2.53	1.03	2.46	1.19	147
North Su NS-2[φ]	215	442	38.8	352	0.91	0.56	1.62	1.04	149
Suzette SZ-5[φ]	249	610	0	33.7	0.63	1.10	0.57	1.24	3.0
Satanic Mills SM-2[φ]	241	455	0	15.3	0.19	0.87	0.21	2.24	7.1

[Ŧ]Douville *et al.*, 1999; [φ]Craddock *et al.*, 2010; [λ]Schmidt *et al.*, 2010. T_{max} indicates the maximum temperature measured during fluid sampling, with the exception of Winter Palace where parentheses indicate T_{max} prior to fluid sampling. Only the sample with lowest [Mg] is shown for the Kemp Caldera vent sites. Sulphate values of < 0 indicate removal by subsurface anhydrite deposition.

Table 3. REE-Y concentrations (ppm) in hydrothermal chimney anhydrite from the East Scotia Ridge and Kemp Caldera

Sample ID	Sample Location	La	Ce	Pr	Nd	Sm	Eu	Gd	Tb	Dy	Ho	Er	Tm	Yb	Lu	Y
East Scotia Ridge																
130-9-S1 (1)	Dog's Head, E2	1.30	2.73	0.39	1.67	0.38	0.10	0.35	0.04	0.24	0.03	0.07	0.01	0.04	0.005	0.87
130-9-S1 (2)	Dog's Head, E2	1.70	3.35	0.47	2.07	0.49	0.10	0.43	0.06	0.28	0.04	0.10	0.01	0.05	0.01	1.09
132-S11	Dog's Head, E2	0.80	1.65	0.24	1.12	0.29	0.03	0.27	0.04	0.18	0.03	0.06	0.007	0.04	0.005	0.71
140-S4-top	Black & White, E9N	2.53	7.65	1.36	7.04	1.82	0.36	1.79	0.21	0.99	0.15	0.28	0.02	0.10	0.01	4.18
142-S5	Ivory Towers, E9S	0.06	0.11	0.02	0.06	0.01	0.05	0.01	0.001	0.007	0.001	0.003	0.000	0.002	0.000	0.04
144-S7	Launch Pad, E9S	0.89	1.78	0.24	0.96	0.19	1.05	0.15	0.02	0.09	0.01	0.04	0.004	0.02	0.003	0.34
Kemp Caldera																
149-S11	Winter Palace	0.02	0.04	0.006	0.04	0.15	0.55	0.83	0.20	1.62	0.33	0.80	0.09	0.48	0.06	7.47
152-S13	Winter Palace	0.01	0.02	0.003	0.02	0.01	0.01	0.04	0.02	0.19	0.05	0.13	0.02	0.09	0.01	1.20
Mid-Atlantic Ridge																
957C-6W-1[a]	TAG-1	0.53	1.05	0.14	0.61	0.15	0.40	0.10	0.02	0.09	0.02	0.03	0.005	0.031	0.005	-
957C-7N-1[a]	TAG-1	0.45	1.05	0.16	0.73	0.18	0.45	0.14	0.02	0.10	0.02	0.03	0.005	0.025	0.003	-
957H-5N-2[a]	TAG-2	0.64	1.32	0.20	0.95	0.33	0.88	0.26	0.04	0.20	0.03	0.06	0.006	0.032	0.003	-
123 ROV-4[b]	Two Boats, 5°S	1.39	2.78	0.40	2.05	0.59	0.13	0.70	0.10	0.53	0.09	0.19	0.02	0.09	0.01	2.81
139-415c[b]	Two Boats, 5°S	0.53	1.26	0.21	1.17	0.35	0.11	0.41	0.05	0.26	0.04	0.07	0.007	0.03	0.003	0.17
Manus Basin																
1188A-7R-1[c]	Snowcap	1.37	3.77	0.60	2.98	0.91	0.31	1.36	0.23	1.59	0.37	1.15	-	1.37	0.24	9.89
1188A-7R-1; #2[d]	Snowcap	0.65	1.98	-	1.68	0.52	0.30	0.76	-	0.65	0.16	0.48	-	0.62	-	-
1188A_7R_1; #19[d]	Snowcap	0.29	1	-	0.8	0.31	0.07	0.46	-	0.35	0.08	0.26	-	0.34	-	-
227_7_R2; #9[d]	North Su	1.39	4.73	-	5.01	1.90	1.20	1.98	-	2.02	0.39	1.04	-	1.16	-	-
227_7_R2; #17[d]	North Su	0.58	1.71	-	1.45	0.61	0.64	0.79	-	0.91	0.18	0.49	-	0.49	-	-
227_7_R2; #18[d]	North Su	0.62	1.72	-	2.98	1.31	0.83	2.55	-	3.64	0.83	2.44	-	2.36	-	-

[a]Humphris, 1998; [b]Schmidt *et al*., 2010; [c]Bach *et al*., 2003; [d]Craddock and Bach, 2010

Table 4. Total REE concentration, REE ratios, and Sr isotope data for anhydrite samples from the East Scotia Ridge and Kemp Caldera. Data for anhydrites sampled from Mid-Atlantic Ridge and Manus Basin hydrothermal sites are also provided for comparison.

	∑REE ppm	**La_{CN} /Yb_{CN}**	**La_{CN} /Nd_{CN}**	**Nd_{CN} /Yb_{CN}**	**Eu_{CN} /Eu^*_{CN}**	**$^{87}Sr/^{86}Sr$**	**[Sr] ppm**	**% SW**
East Scotia Ridge								
E2 (Dog's Head 130-1)	7.34	21.6	1.50	14.4	0.85	0.70678	1520	55
E2 (Dog's Head 130-2)	9.13	20.9	1.55	13.5	0.63	-	-	-
E2 (Dog's Head 132)	4.75	14.3	1.37	10.4	0.35	0.70816	1050	82
E9 North (B&W)	24.3	17.1	0.69	24.7	0.61	0.70607	1310	2
E9 South (Ivory Tower)	0.33	16.6	1.78	9.31	13.9	0.70876	3330	73
E9 South (Launch Pad)	5.44	26.1	1.79	14.6	18.8	0.70669	2170	14
Kemp Caldera								
Winter Palace (149)	5.19	0.03	1.05	0.03	3.84	0.70658	2170	-
Winter Palace (152)	0.61	0.09	1.43	0.07	1.87	0.70886	3070	53
Mid-Atlantic Ridge								
TAG-1 (957C-6W-1)[a]	3.18	11.4	1.66	6.86	9.50	-	-	-
TAG-1 (957C-7N-1)[a]	3.56	12.2	1.21	10.1	8.55	0.70716	1490	68
TAG-2 (957H-5N-2)[a]	4.95	13.4	1.30	10.3	8.93	-	-	-
Two Boats (123 ROV-4)[b]	9.04	10.1	1.30	7.78	0.62	-	-	-
Two Boats (139-415c)[b]	4.52	12.4	0.88	14.1	0.85	-	-	-
Manus Basin								
Snowcap (1188A-7R-1)[c, d]	16.3	0.67	0.88	0.76	0.87	0.70835	3430	84
Snowcap (1188A-7R-1; #2)[e]	7.80	0.70	0.74	0.95	1.48	0.70856	2690	-
Snowcap (1188A_7R_1; #19)[e]	3.96	0.57	0.70	0.82	0.57	-	-	-
North Su (227_7_R2; #9)[e]	20.8	0.80	0.53	1.51	1.90	-	2255	-
North Su (227_7_R2; #17)[e]	7.85	0.79	0.77	1.03	2.85	0.70627	3650	-
North Su (227_7_R2; #18)[e]	19.3	0.18	0.40	0.44	1.38	0.70675	2748	-

[a]Humphris *et al*., 1998; [b]Schmidt *et al*., 2010; [c]Bach *et al*., 2003; [d]2005; [e]Craddock and Bach, 2010

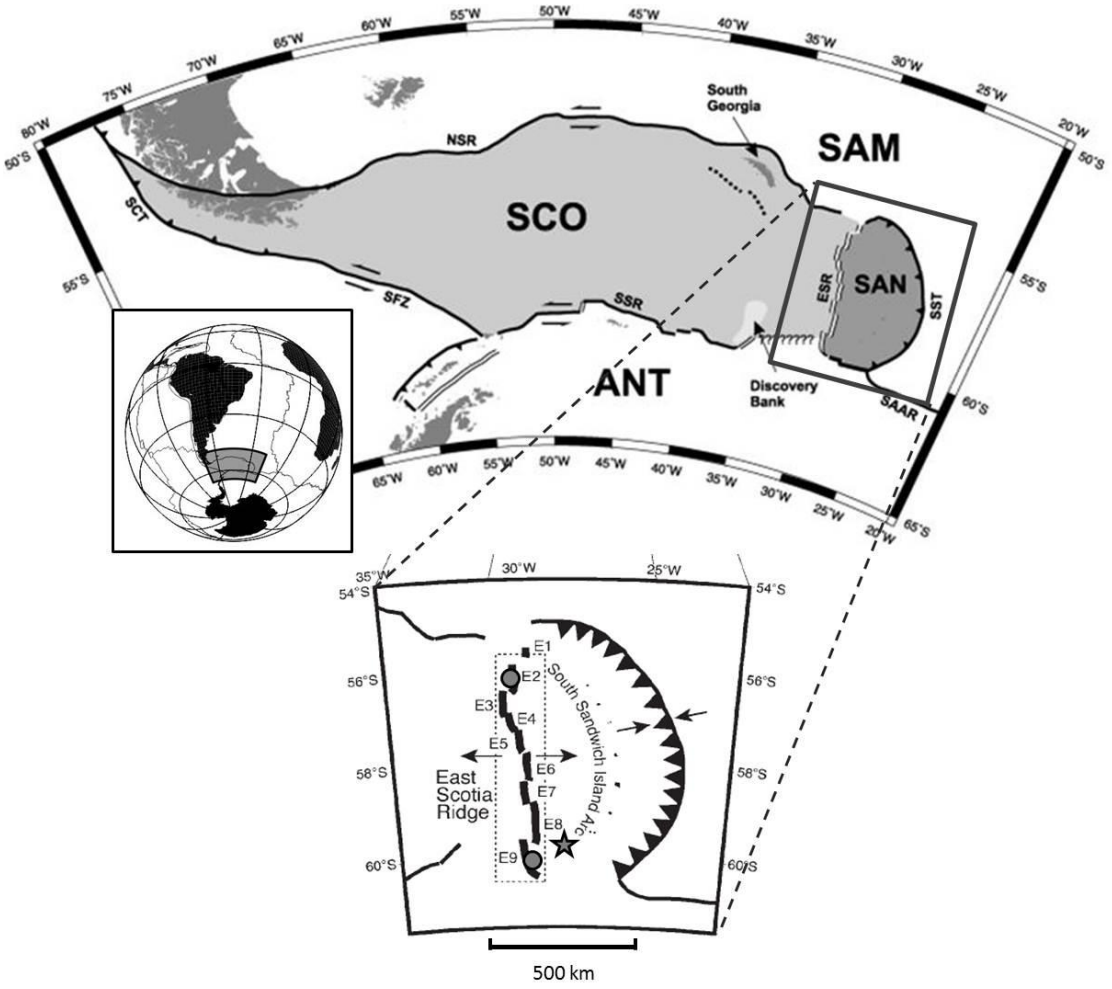

Figure 1. Location of the East Scotia Ridge (ESR) and Kemp Caldera in the Scotia Sea, in relation to the South American plate (SAM), the Antarctic plate (ANT), the Scotia plate (SCO) and the Sandwich plate (SAN). ESR segments E1 – E9 are labelled. Confirmed sites of hydrothermal activity are indicated by grey circles (E2 and E9) and by the grey star at the base of the South Sandwich Island Arc (Kemp Caldera). SFZ: Shackleton Fracture Zone, NSR: North Scotia Ridge, SSR: South Scotia Ridge, SCT: Southern Chile Trench, SST: South Sandwich Trench and SAAR: South American-Antarctic Ridge. Adapted from Rogers *et al*. (2012); Thomas *et al*. (2003); Fretzdorff *et al*. (2002).

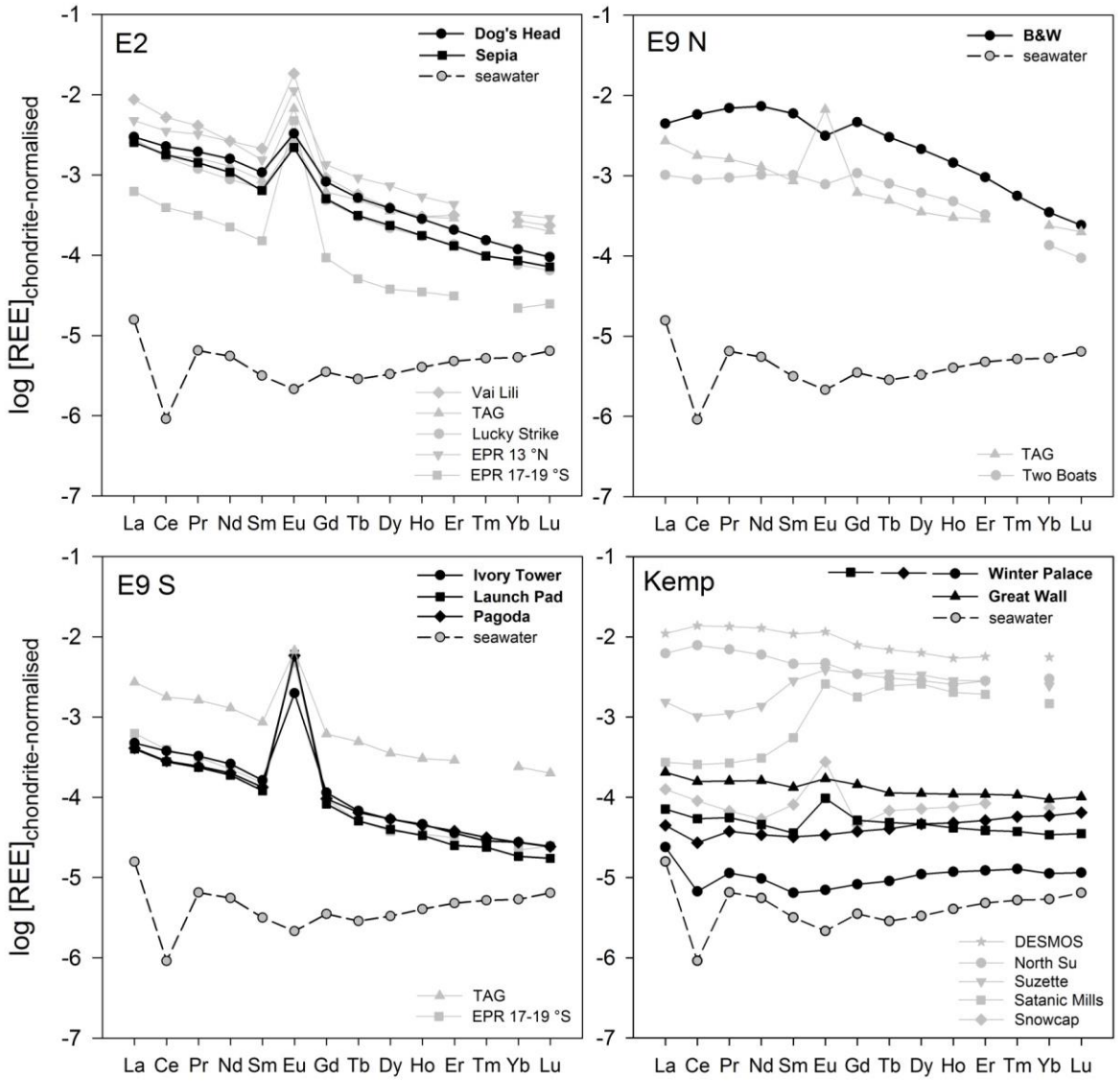

Figure 2. Chondrite-normalised REE patterns in endmember vent fluids from E2 (Dog's Head and Sepia), E9 North (Black & White) and E9 South (Ivory Tower, Launch Pad, Pagoda) on the East Scotia Ridge, and in sampled fluids from Kemp Caldera (Winter Palace and Great Wall). Patterns for a typical mid-ocean ridge hydrothermal fluid (TAG), as well as for other vent sites that exhibit similar REE_{CN} patterns to sites from the ESR, are also shown. These data are from: Douville *et al*. (1999) (Lau Basin: Vai Lili; MAR: TAG, Lucky Strike; EPR: 13 °N, 17-19 °S); Schmidt *et al*. (2010) (MAR: Two Boats); Craddock *et al*. (2010) (Manus Basin: DESMOS, North Su, Suzette, Satanic Mills, Snowcap). Seawater data (Circumpolar Deep Water) were determined in this study; see also Hathorne *et al*. (2012).

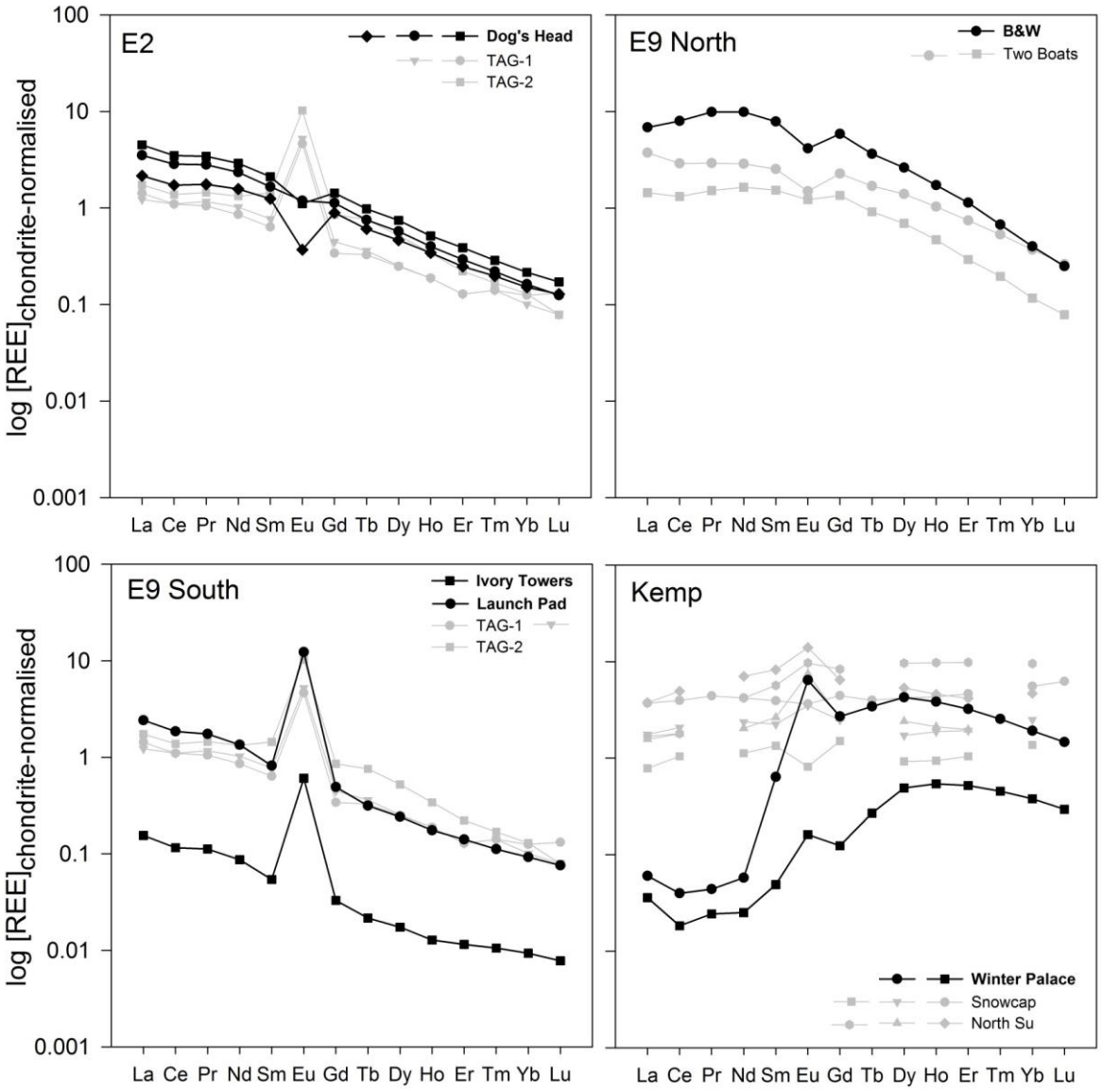

Figure 3. Chondrite-normalised REE distribution patterns for chimney anhydrite from E2 (Dog's Head), E9 North (Black & White), E9 South (Launch Pad and Ivory Towers), and Kemp Caldera (Winter Palace). Data for other vent sites are from: Humphris (1998) (TAG), Schmidt *et al*. (2010) (Two Boats), Bach *et al*. (2003) (Snowcap) and Craddock and Bach (2010) (Snowcap and North Su).

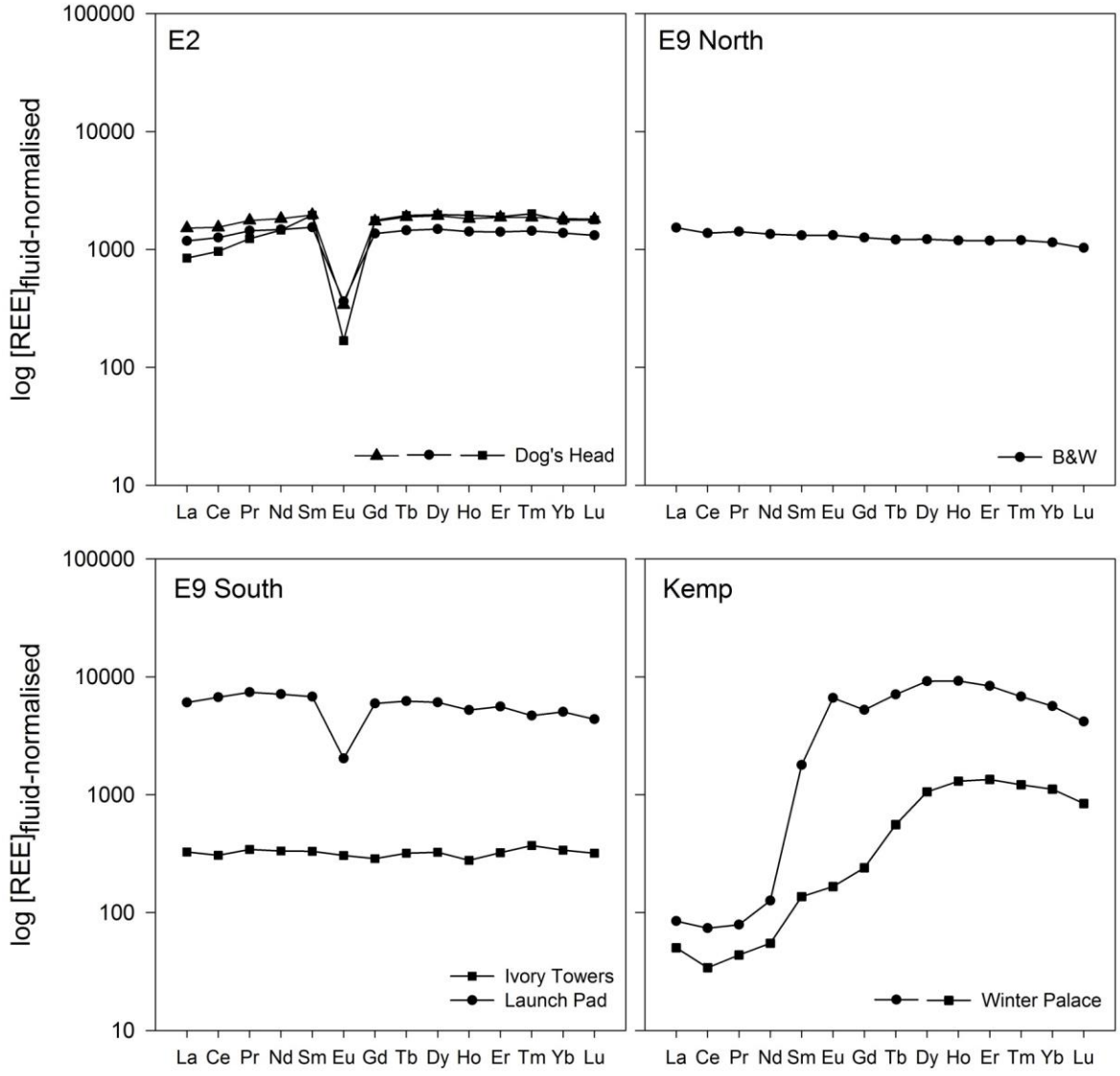

Figure 4. Vent fluid-normalised REE fractionation patterns for chimney anhydrite from E2 (Dog's Head), E9 North (Black & White), E9 South (Ivory Tower and Launch Pad), and Kemp Caldera (Winter Palace). Samples from the ESR are normalised to the endmember vent fluid composition; samples from Kemp Caldera are normalised to the composition of the vent fluid with lowest [Mg].

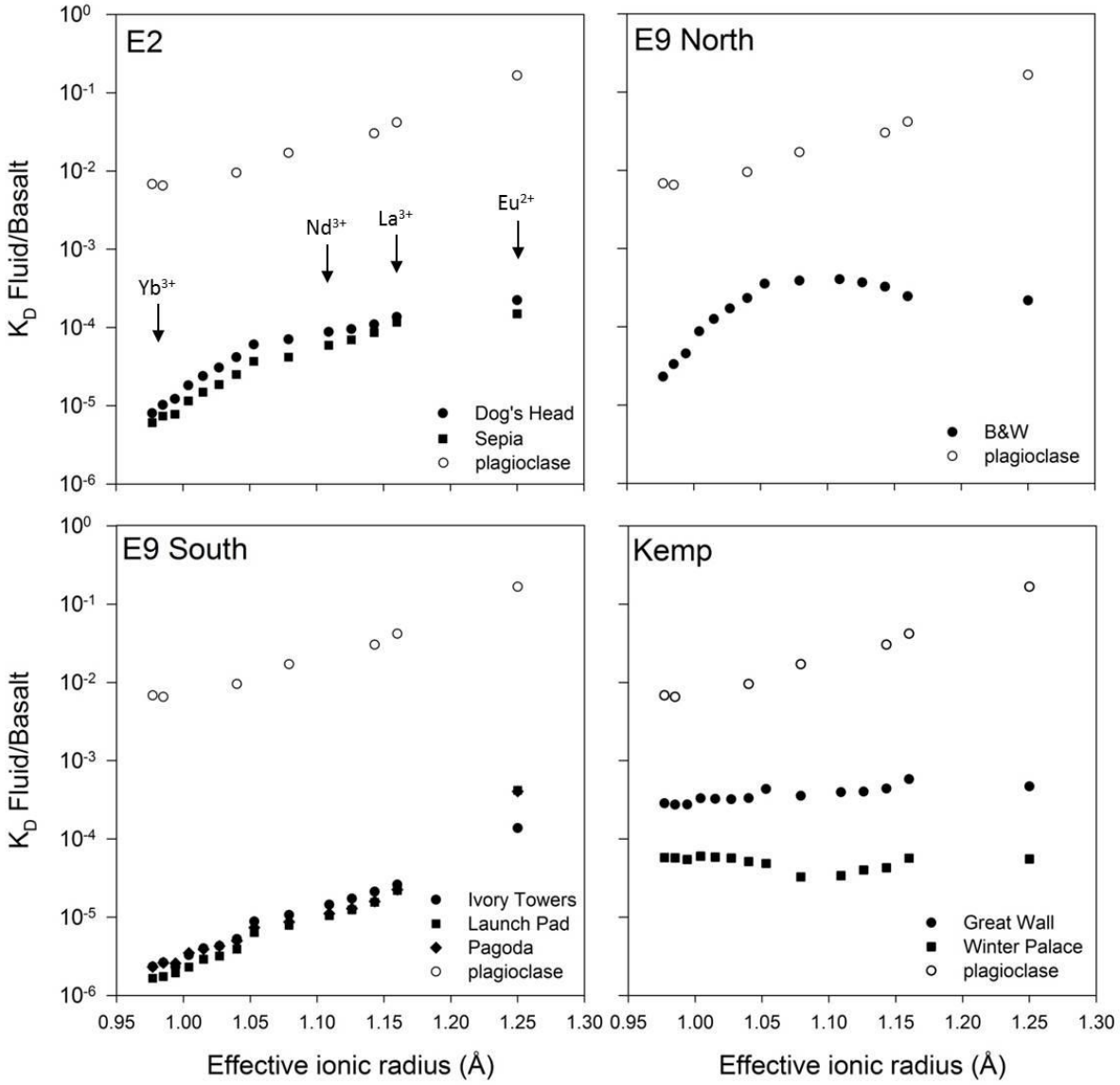

Figure 5. Distribution of the REEs between basalt and hydrothermal fluids, presented in terms of the partition coefficient, K_D, versus effective ionic radius (Å) in octahedral coordination (Shannon, 1976). Endmember and sampled (lowest Mg) fluids are used for ESR and Kemp, respectively. Data for E2 and E9 basalts are from Leat *et al*. (2000; 2004); Fretzdorff *et al*. (2002). Also shown are K_D values for the REEs in plagioclase during magma segregation (Phinney and Morrison, 1990).

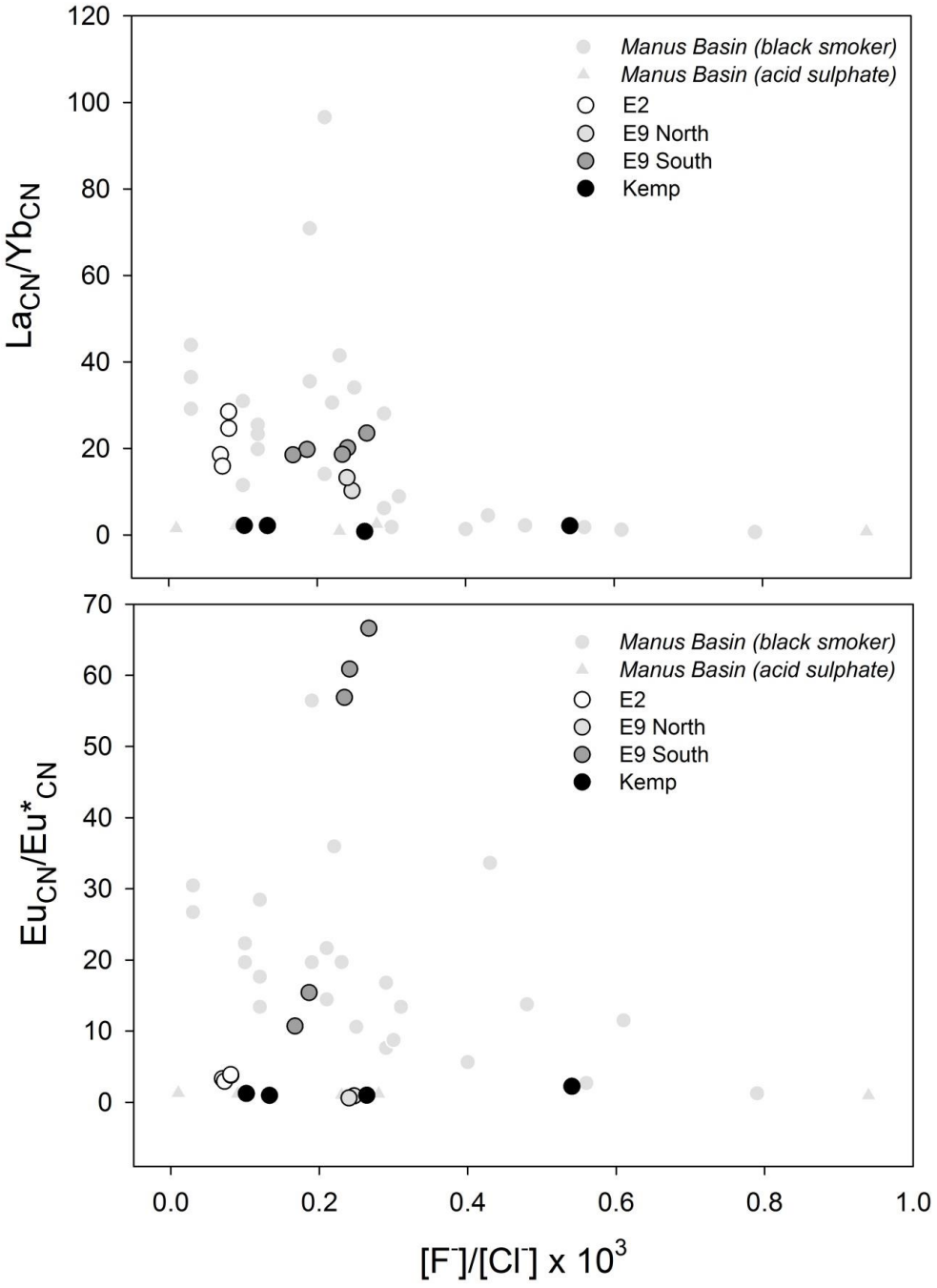

Figure 6. Relationship between (a) La_{CN}/Yb_{CN} and (b) Eu_{CN}/Eu^*_{CN} and fluoride/chloride ratio in sampled hydrothermal fluids from the East Scotia subduction zone system. Only low Mg (< 8 mM) values are included for ESR fluids, alongside sampled (Mg > 43 mM) fluids for Kemp Caldera. Data for vent fluids from the Manus Basin (black smoker- and acid sulphate-type) are also shown for comparison (Craddock *et al.*, 2010).

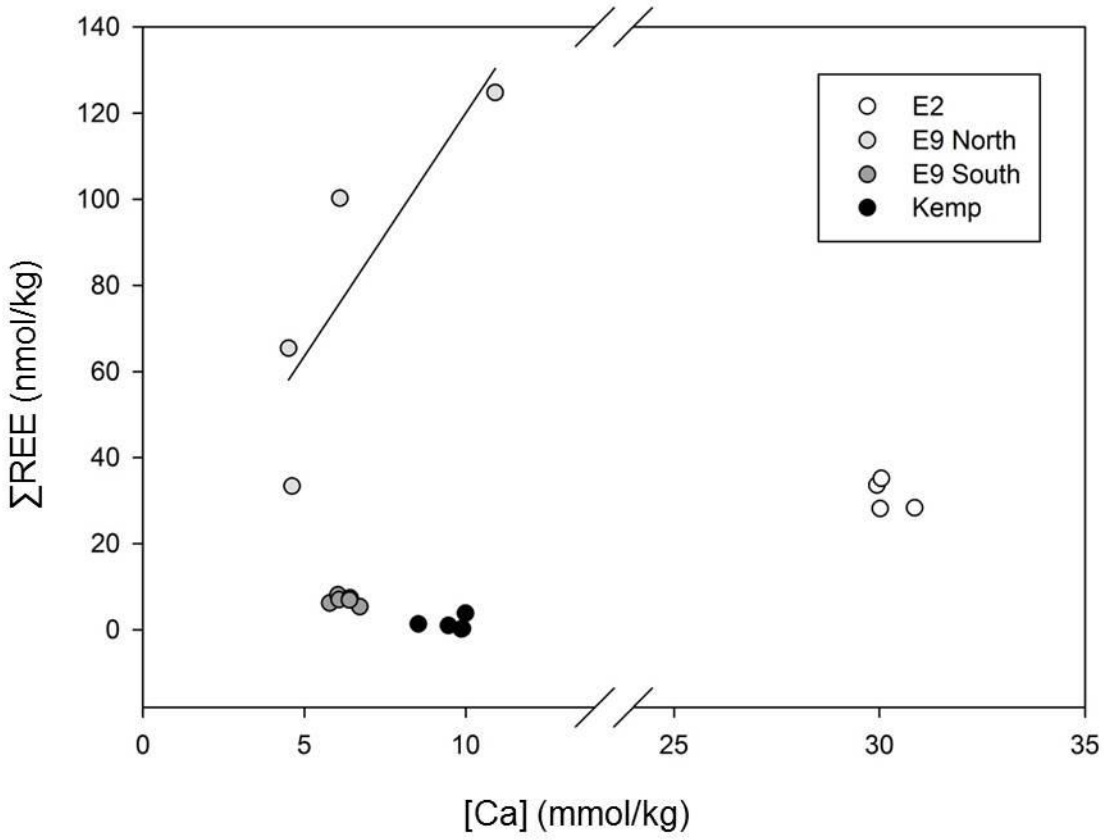

Figure 7. Total REE concentration (∑REE) versus Ca concentration in sampled fluids from E2, E9 North, E9 South and Kemp Caldera. Fluids recovered from E9 North (including two fluids for which no 'dregs' were available for analysis, in addition to the fluids reported in Table 1) exhibit a positive correlation between ∑REE and [Ca], indicated by the trend line ($R^2 = 0.72$).

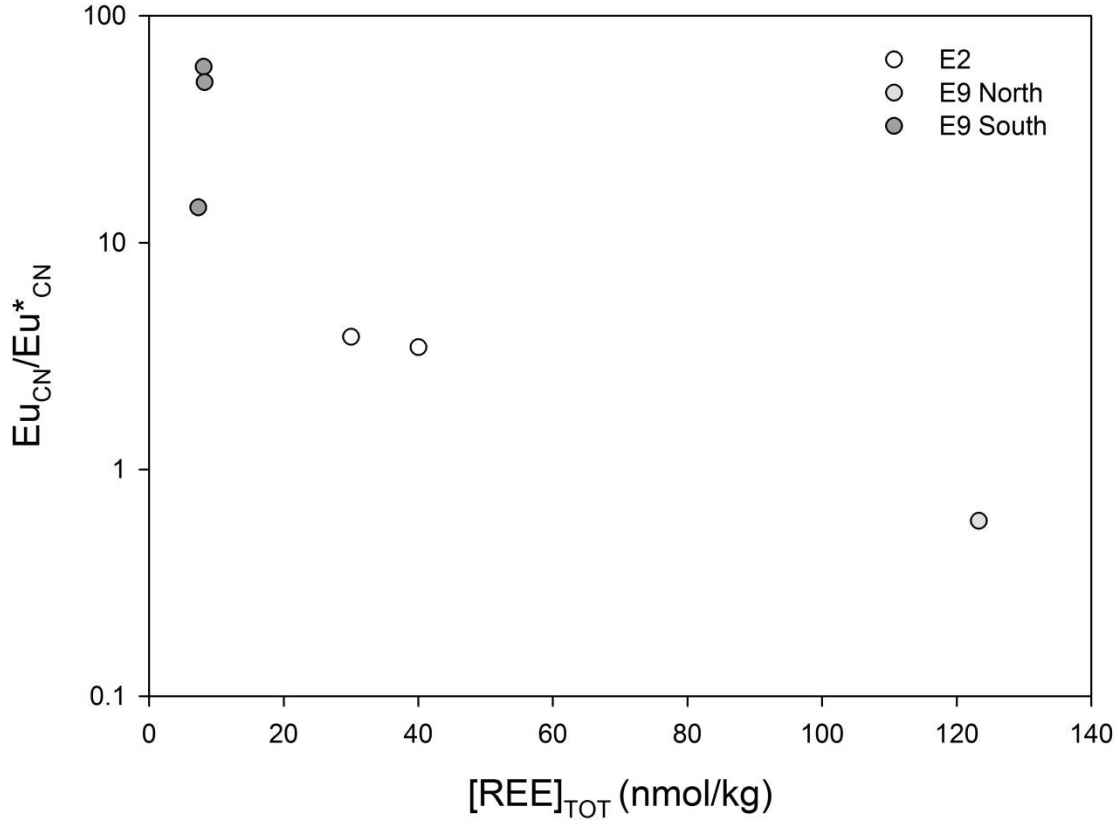

Figure 8. Chondrite-normalised Eu anomaly (Eu_{CN}/Eu^*_{CN}) versus total REE concentration in endmember fluids from the ESR.